

RADIATIONAL PARAMETERIZATION FOR THE FNWC
PRIMITIVE EQUATION MODEL USING DATA
OVER THE OCEANS FOR 16 APRIL 1974

William Thurman Meyers

DUDLEY KNOX LIBRARY
NAVAL POSTGRADUATE SCHOOL
MONTEREY, CALIFORNIA 93940

NAVAL POSTGRADUATE SCHOOL

Monterey, California



THESIS

RADIATIONAL PARAMETERIZATION FOR THE FNWC
PRIMITIVE EQUATION MODEL USING DATA
OVER THE OCEANS FOR 16 APRIL 1974

by

William Thurman Meyers

September 1975

Thesis Advisor:

F. L. Martin

Approved for public release; distribution unlimited.

-1696 56

REPORT DOCUMENTATION PAGE		READ INSTRUCTIONS BEFORE COMPLETING FORM
1. REPORT NUMBER	2. GOVT ACCESSION NO.	3. RECIPIENT'S CATALOG NUMBER
4. TITLE (and Subtitle) Radiational Parameterization for the FNWC Primitive Equation Model Using Data Over the Oceans for 16 April 1974.		5. TYPE OF REPORT & PERIOD COVERED Master's Thesis September 1975
7. AUTHOR(s) William Thurman Meyers		6. PERFORMING ORG. REPORT NUMBER
9. PERFORMING ORGANIZATION NAME AND ADDRESS Naval Postgraduate School Monterey, California 93940		8. CONTRACT OR GRANT NUMBER(s)
11. CONTROLLING OFFICE NAME AND ADDRESS Naval Postgraduate School Monterey, California 93940		10. PROGRAM ELEMENT, PROJECT, TASK AREA & WORK UNIT NUMBERS
14. MONITORING AGENCY NAME & ADDRESS (if different from Controlling Office) Naval Postgraduate School Monterey, California 93940		12. REPORT DATE September 1975
		13. NUMBER OF PAGES 130
		15. SECURITY CLASS. (of this report) Unclassified
		15a. DECLASSIFICATION/DOWNGRADING SCHEDULE
16. DISTRIBUTION STATEMENT (of this Report) Approved for public release; distribution unlimited.		
17. DISTRIBUTION STATEMENT (of the abstract entered in Block 20, if different from Report)		
18. SUPPLEMENTARY NOTES		
19. KEY WORDS (Continue on reverse side if necessary and identify by block number) Cloud Parameterization Tropospheric Heat Balance Model Radiation Budget		
20. ABSTRACT (Continue on reverse side if necessary and identify by block number) The radiational model used in this study computes the planetary albedo and absorption of solar insolation by the ocean's surface and by atmospheric layers for the primitive equation model of FNWC. Large-scale cloud parameterization in several layers was utilized in these computations. Solar insolation disposition was computed from the water-mass and the cloud amounts over each grid point. Long-wave cooling effects were computed using emissivity		

formulas after Sasamori at the earth's surface and over the same layers, and were also found to be dependent upon the cloud parameterization.

Two forms of the cloud parameterization were tested using FNWC data over the oceanic gridpoints for 16 April 1974. The objective was to determine the parameterization which better verified the radiational balance as a function of latitude when compared with satellite climatology at the top of the atmosphere for the same general data-period in 1969 (after Raschke, et al, 1973). The better verification resulted with the smaller cloud parameterization values.

Radiational Parameterization for the FNWC
Primitive Equation Model Using Data
Over the Oceans for 16 April 1974

by

William Thurman Meyers
Lieutenant, United States Navy
B.S., North Texas State University, 1965

Submitted in partial fulfillment of the .
requirements for the degree of

MASTER OF SCIENCE IN METEOROLOGY

from the
NAVAL POSTGRADUATE SCHOOL
September 1975

ABSTRACT

The radiational model used in this study computes the planetary albedo and absorption of solar insolation by the ocean's surface and by atmospheric layers for the primitive equation model of FNWC. Large-scale cloud parameterization in several layers was utilized in these computations. Solar insolation disposition was computed from the water-mass and the cloud amounts over each gridpoint. Long-wave cooling effects were computed using emissivity formulas after Sasamori at the earth's surface and over the same layers, and were also found to be dependent upon the cloud parameterization.

Two forms of the cloud parameterization were tested using FNWC data over the oceanic gridpoints for 16 April 1974. The objective was to determine the parameterization which better verified the radiational balance as a function of latitude when compared with satellite climatology at the top of the atmosphere for the same general data-period in 1969 (after Raschke, et al, 1973). The better verification resulted with the smaller cloud parameterization values.

TABLE OF CONTENTS

I.	INTRODUCTION - - - - -	18
II.	DATA PREPARATION - - - - -	21
A.	INITIAL DATA FIELDS- - - - -	21
B.	INTERPOLATIVE PROCESSING TO K-LEVELS IN RADIATIVE SOUNDINGS - - - - -	27
1.	Temperature Profiles - - - - -	27
2.	Moisture Profiles- - - - -	27
3.	Pressure-Scaled Absorber Masses- - - - -	29
C.	CLOUD PARAMETERIZATION - - - - -	29
D.	CLOUD-AREA COVERAGES - - - - -	31
III.	TERRESTRIAL RADIATION- - - - -	33
A.	THEORETICAL AND EMPIRICAL BASIS- - - - -	33
B.	NET FLUX FORMULATION - - - - -	34
1.	At Level $k=10$ - - - - -	34
2.	Net Flux F_6^* - - - - -	36
3.	Net Flux F_2^* - - - - -	36
C.	APPLICATIONS TO HEAT BALANCE COMPUTATIONS- - - - -	38
1.	At Upper and Lower Boundaries- - - - -	38
2.	Intermediate Levels- - - - -	38
D.	STATISTICAL RESULTS AND COMPARISONS- - - - -	39
1.	Net Flux $F_{10}^*(0,0)$ - - - - -	39
2.	Modification of F_{10}^* for Cloudiness CL_1, CL_2 - - - - -	42
E.	COMPARISONS OF FF2 WITH SATELLITE CLIMATOLOGY- - - - -	44

	F. COMPARISONS OF CROSS-SEASONAL RESULTS OF F_{10}^* - - - - -	46
IV.	SOLAR RADIATION- - - - -	49
	A. PARTITION OF SOLAR INSOLATION- - - - -	49
	B. DISPOSITION OF F(S) INSOLATION - - - - -	52
	1. Clear Sky Case - - - - -	53
	2. Cloudy Sky Cases - - - - -	53
	3. Composite F(S) Insolation- - - - -	54
	C. DISPOSITION OF F(A) INSOLATION - - - - -	56
	1. Clear Sky Case (0,0) - - - - -	56
	2. Cloudy Cases - - - - -	57
	3. Composite F(A) Layer-Absorptions and Surface-Absorption Insolation- - - - -	61
	4. Absorptivity (ABA) by Layers - - - - -	63
	D. ALBEDO (ALB) OF THE EARTH-TROPOSPHERE SYSTEM - - - - -	63
	E. COMPOSITE ABSORPTIVITY (ABG) BY THE EARTH-SURFACE; COMPOSITE ATMOSPHERIC TRANSMISSIVITY (ATRAN) - - - - -	64
	1. Absorptivity (ABG) of Earth - - - - -	64
	2. Transmissivity (ATRAN) of the Troposphere- - - - -	64
	3. Computational Check- - - - -	65
	F. STATISTICAL ANALYSIS - - - - -	65
	1. Clear Sky Cases- - - - -	66
	2. Statistical Relationships Between ALB, ABA, and ATRAN in the Cloudy and Clear Sky Cases- - - - -	67
	G. ALBEDO COMPARISONS WITH PUBLISHED RESULTS-	71

V.	SENSIBLE AND LATENT HEAT TRANSPORT AT THE SEA-AIR INTERFACE- - - - -	75
A.	GENERAL PURPOSE- - - - -	75
B.	WINDSPEED COMPUTATION IN THE TURBULENT FLUX MODEL - - - - -	75
C.	SENSIBLE HEAT TRANSPORT- - - - -	77
D.	EVAPORATIVE HEAT TRANSPORT - - - - -	80
E.	TURBULENT HEAT TRANSPORTS OVER AN ICE-COVERED OCEAN- - - - -	82
F.	LARGE-SCALE TURBULENT HEAT FLUX ACROSS THE SEA-AIR INTERFACE- - - - -	82
VI.	LATITUDINAL CROSS-SECTIONAL DEPICTION OF THE HEAT-BALANCE COMPUTATIONS- - - - -	85
A.	GENERAL- - - - -	85
B.	GEOGRAPHICAL REPRESENTATION OF THE HEAT-BALANCE DISTRIBUTION- - - - -	85
C.	EXPLANATION OF SYMBOLIC TERMS- - - - -	86
	1. Cross-Section at Level k=2 (Fig. 6)- -	86
	2. Cross-Section at Layer (2,6) - - - - -	86
	3. Cross-Section at Layer (6,10)- - - - -	89
	4. Cross-Section at Air-Sea Interface (k=10) - - - - -	90
D.	LATITUDINAL CROSS-SECTIONS OF THE VERTICAL HEAT BALANCE FOR 16 APRIL 1974- -	90
VII.	THE LATITUDINAL DISTRIBUTION OF RADIATIONAL BALANCE TERMS OF THE OCEAN-ATMOSPHERE SYSTEM -	101
A.	GENERAL- - - - -	101
B.	EARTH-TROPOSPHERE SYSTEM RADIATIONAL BALANCE SUMMARY- - - - -	102
C.	CROSS-SEASONAL EFFECTS - - - - -	111
D.	COMPARISONS OF NET FLUX AT THE TOP OF THE MODEL ATMOSPHERE WITH SATELLITE OBSERVATIONS - - - - -	112

VIII.	ZONALLY-AVERAGED TROPOSPHERIC AND OCEANIC HEAT BUDGETS FOR 16 APRIL 1974 - - - - -	119
A.	THE TROPOSPHERIC HEAT BUDGET - - - - -	119
B.	LATITUDINALLY-AVERAGED HEAT BUDGET OF THE OCEAN - - - - -	122
IX.	CONCLUSIONS- - - - -	125
	LIST OF REFERENCES- - - - -	127
	INITIAL DISTRIBUTION LIST - - - - -	130

LIST OF TABLES

Table

I	a. Example of a typical FNWC sounding for gridpoint (1,1)- - - - -	24
	b. Example of the corresponding radiative sounding with temperature and mixing ratio listed at k-levels and also water vapor and CO ₂ absorber masses, cloud amounts CL(1) ² and CL(2) where applicable in the example sounding - - - - -	25
II.	Sample listing of gridpoint values of the terrestrial radiation fluxes computed at gridpoint (1,1)- - - - -	41
III.	Statistical cross-seasonal comparison for the six month period of 16 January - 16 July 1974, of the downward flux at the surface as given by the Brunt formulation for both the 2/3-CL and full-CL parameterization - - - - -	42
IV.	Statistical cross-seasonal comparison for the six month period of 16 January - 16 July 1974 of the net flux at the surface, F_{10}^* , for the 2/3-CL parameterization - - - - -	44
V.	Comparison of net flux to space, F_2 , as found by this study for both the 2/3-CL case and the full-CL case, and by Raschke et al (1973) using NIMBUS III heat budget studies. Composite CL amounts for both cases are also included- - - - -	47
VI.	Cross-seasonal comparison for the six month period of 16 January - 16 July 1974, of the net flux at the surface, F_{10}^* , and the composite cloud cover for the 2/3-CL parameterization - - - - -	48
VII.	Sample listing of gridpoint values of the cloud-weighted $F(S)$ insolation penetrating the earth's surface computed at gridpoint (1,1)- - - - -	56

VIII.	Sample listing of gridpoint values of the cloud-weighted $F(A)$ insolation subject to absorption by atmospheric water-vapor and CO_2 , computed at gridpoint (1,1) - - - - -	62
IX.	Comparison of planetary albedo as found by this study for both the 2/3-CL case and the full-CL case and by Raschke et al (1973) based upon NIMBUS III measurements. Also included are the globally-weighted mean values and the composite cloud amounts for both cloud cases - - - - -	73
X.	Cross-seasonal comparison for the six month period of 16 January - 16 July 1974, of the ocean-troposphere net radiation R_s for both the 2/3-CL and the full-CL parameterization - - - - -	115
XI.	Cross-seasonal comparison for the six month period of 16 January - 16 July 1974, of the surface net radiation R for both the 2/3-CL and the full-CL parameterization - - - - -	116
XII.	Cross-seasonal comparison for the six month period of 16 January - 16 July 1974, of the atmospheric-net radiation loss-rate R_a for both the 2/3-CL and the full-CL parameterization - - - - -	117
XIII.	Comparison of the ocean-troposphere net radiation R_s and RNMOD as found by this study for both 2/3-CL and the full-CL cases and RNRAS by Raschke et al (1973)- - - -	118
XIV.	Comparison of the zonally-averaged values of $(E + H_T)$ as found by this study - - - - -	119

LIST OF FIGURES

Figure

1.	FNWC polar stereographic grid meridians (lines 1,2,3 and 4) selected for study - - - -	22
2.	Five-layer radiative sounding used in this study -	26
3.	Schematic representation of F(A) insola- tion disposition in the case of two overcast layers- - - - - - - - - - - - - - - - - - - -	59
4.	Section of FNWC polar stereographic grid illustrating the method of obtaining contour gradients in the vicinity of a gridpoint- - - - - - - - - - - - - - - - - - - -	79
5.	Schematic representation of the distri- bution of convergence of sensible and latent heat- - - - - - - - - - - - - - - - - - - -	83
6.	Key to meridional cross-sections for Figs. 7...10 -	92
7.	125W longitudinal cross-section. Two- thirds cloud model -	
a.	Tropical section -	93
b.	Higher latitude section- - - - - - - - - - - - - - - - - - - -	94
8.	170W longitudinal cross-section. Two- thirds cloud model -	
a.	Tropical section -	95
b.	Higher latitude section- - - - - - - - - - - - - - - - - - - -	96
9.	145E longitudinal cross-section. Two- thirds cloud model -	
a.	Tropical section -	97
b.	Higher latitude section- - - - - - - - - - - - - - - - - - - -	98

10.	35W longitudinal cross-section. Two-thirds cloud model - - - - -	
a.	Tropical section - - - - -	99
b.	Higher latitude section- - - - -	100
11.	Key to zonally-averaged radiational cross-section for Figs. 12(a,b) and 13(a,b)- - - - -	103
12.	Zonally-averaged radiational cross-section for the two-thirds cloud model case - - - - -	
a.	Tropical latitude section- - - - -	104
b.	Mid to high latitude section - - - - -	105
13.	Zonally-averaged radiational cross-section for the full cloud model case- - - - -	
a.	Tropical latitude section- - - - -	106
b.	Mid to high latitude section - - - - -	107
14.	Radiational balance at the tropopause (R_a), in the atmospheric column between $k \leq 2$ and $k = 10(R_a)$, and at the ocean surface (R_s) of both the two-thirds cloud case and the full cloud case for 16 April 1974 - - - - -	110
15.	Tropospheric heat budget disposition of both the two-thirds cloud case model and the full cloud case model for 16 April 1974- - - - -	121
16.	Surface heat budget disposition of both the two-thirds cloud case model and the full cloud case model for 16 April 1974- - - - -	124

LIST OF SYMBOLS AND ABBREVIATIONS

$A(m,n)$	- solar insolation absorbed in the layer (m,n)
$\bar{a}(m,n)$	- Manabe-Möller absorptivity function
a^*	- turbulent transfer coefficient
ABA	- absorptivity of the troposphere
ABG	- fractional absorptivity of solar insolation by earth's surface
ALB	- earth-atmospheric system albedo
ATRAN	- transmissivity of the troposphere
B_k	- Stefan-Boltzmann blackbody flux at T_k
BALB	- 24-hour averaged radiational balance at earth's surface
$BALk_1k_2$	- 24-hour averaged radiational balance for layer (k_1, k_2)
BALT	- 24-hour averaged radiational balance at tropopause
BBB	- ice conduction coefficient
C	- carbon dioxide layer absorber mass
$\text{cal cm}^{-2} \text{ min}^{-1}$	- calories per centimeter squared per minute
CL	- total opaque cloud cover
CL(I)	- fractional cloud amount for layer: I = 1 in 600 to 400 mb; I = 2 in 900 to 800 mb
CL'(I)	- two-thirds of cloud amount CL(I)
E	- East longitude; evaporation
e_x	- vapor pressure at top of constant flux layer
F(A)	- solar insolation subject to water vapor absorption only

FADJ	- total incoming insolation at top of atmosphere
F_d	- net downward flux at the earth
FF2	- total long-wave flux to space at level $k=2$
$F_{k_1 k_2}$	- net infrared flux divergence between level k_1 and k_2
F_k^*	- net infrared flux at level k
FNWC	- Fleet Numerical Weather Central
F(S)	- solar insolation subject to Rayleigh scattering only
F2(RAS)	- total long-wave flux to space at level $k=0$ based upon NIMBUS III measurements by Raschke et al (1973)
g	- gravity = $9.8067 \text{ m sec}^{-2}$
h	- hour angle
H	- height of homogeneous atmosphere; 24-hour averaged hour angle
H_T	- sensible heat transport
HICE	- heat conduction into ice
I	- abscissa grid location
IA10(m,n)	- solar insolation absorbed at surface with cloud condition (m,n)
IS10(m,n)	- solar insolation at surface subject to Rayleigh scatter with cloud condition (m,n)
J	- ordinate grid location
k	- pressure level used in this study equal to 10σ
K^*	- eddy turbulent transfer coefficient
L	- latent heat of vaporization
$ly \text{ min}^{-1}$	- langleys per minute
M	- water-vapor mass path length

N	- North latitude
P	- pressure
P_k	- pressure in millibars (mb) at level k
q_k	- mixing ratio at level k
q_{s_k}	- saturated mixing ratio at level k
QAVE	- 24-hour averaged insolation at the tropopause
r	- Bowen ratio
R	- correlation coefficient; net radiation balance at the surface
R_a	- mean radiative cooling rate in troposphere
R_d	- gas constant per gram of dry air
REF	- total insolation reflected back to space
REFA	- F(A) insolation reflected back to space
REFS	- F(S) insolation reflected back to space
R.H.	- relative humidity
RN	- total flux to space based upon NIMBUS III measurements by Raschke et al (1973)
RNMOD	- solar insolation minus outgoing terrestrial flux FF2 crossing at level k=2
R_s	- mean radiative energy gain (loss) rate at ocean-troposphere system
S	- South latitude; effective solar constant
S_a	- heat storage term for the troposphere
S_o	- heat storage in the ocean mass
S_t	- Stephan-Boltzmann constant
T_k	- temperature at level k
T_o	- freezing point of sea water
TRAN	- total insolation incident at the earth's surface

T_x	- temperature at the top of constant flux layer
U	- water-vapor layer absorber mass
V_g	- geostrophic windspeed
V_s	- surface windspeed
W	- West latitude
$W(m,n)$	- cloud fractional weight for cloud condition (m,n)
Z	- Zenith angle
Z_k	- height at level k
$\alpha(G)$	- surface albedo
$\alpha(R)$	- Rayleigh clear sky albedo
γ_c	- critical lapse rate
δ	- solar declination angle
ϵ_{wc}	- emissivity due to water and carbon dioxide absorber mass at indicated layer
θ_k	- potential temperature at level k
Λ	- longitude
π	- surface pressure; $\pi = 3.1416$
ρ	- density
σ	- sigma pressure level used by FNWC, normalized to surface pressure
ϕ	- latitude

ACKNOWLEDGEMENT

The author wishes to express his appreciation to his wife, Raynelle, for her patience, encouragement and support as well as the typing of the first draft of this thesis.

Appreciation is also expressed to the author's thesis advisor, Professor F. L. Martin, for his suggestions, advice, guidance and support in this research.

Further appreciation is expressed to Mr. Russell D. Schwanz for his programming assistance.

I. INTRODUCTION

This thesis is a study of a radiative heating parameterization for use in the Fleet Numerical Weather Central (FNWC) prediction system. The study has as a primary objective, the analysis of the radiational and heat balance of the ocean-atmosphere system utilizing FNWC gridded data-fields at constant pressure levels for 16 April 1974. The gridpoint data were selected along four oceanic meridians, three in the Pacific and one in the Atlantic, with most of the gridpoints located in the Northern Hemisphere (Fig. 1).

The specification of amounts of clouds in two designated layers has the most influence on the radiative-model dispositions (short- and long-wave). The initial specification of the fractional amounts of CL(1) and CL(2) are based on large-scale formulations developed by Smagorinsky (1960) and used in a similar study based on the data day 16 January 1974 by Spaeth (1975).

The governing equations of the radiational transfer of the model have been derived by Martin (1972, 1974), who modified both the solar and terrestrial radiation transfers to respond to the presence of clouds. These clouds were of specified amounts in the two layers, one of which is a mid-level cloud and the other a low-level cloud. The radiational model in use here has similarities to those in use in UCLA and NCAR General Circulation models.

The physical description of the radiative model may be applied to any scale of analysis for which there is adequate resolution of the temperature and moisture data in the vertical. In the horizontal, the reliability of the data used here is consistent with that of the FNWC analysis to grid-points, and is typically reported to the nearest tenth of a degree with regard to temperature and dew point. The radiational computations made here are applied to FNWC gridpoints and are designed to make a one-hour forward-time step applicable to the FNWC primitive equation forecast model, with special adaptations to their σ -levels.

The Smagorinsky (1960) cloud-specification of CL(1) and CL(2) when used with the model of this study resulted in global albedo estimates that were too high as compared to the satellite data of Raschke (1973), thus leading to underestimates of the net radiative balance at the top of the atmosphere and at the ocean surface. This problem suggested the reduced cloud-amounts model formulated by Spaeth (1975) and used in this study.

The comparative results afforded by the 2/3-CL parameterization gave reasonably close agreement with the radiative climatology of Raschke et al (1973), for the NIMBUS III period 1-15 May 1969. Oceanic and tropospheric balances were computed for both sets of cloud conditions (full-CL and 2/3-CL) for 16 April 1974. It was also necessary to augment the purely radiative model by including a turbulent

boundary-layer model for sensible and latent heat transports over the ocean as adapted from Kaitala (1974).

The radiation package results computed with the 2/3-CL cloud model compared very favorably with satellite climatology, though only one data day (16 April 1974) was used as representative of mid-April soundings over the ocean, both for the model and the Raschke climatology. However, the latter was based on the data period 1-15 May 1969.

The major effect noted by the use of the 2/3-CL as contrasted with full-CL parameterization was the reduction in global albedo and the resulting greater contribution to the surface net heating rates. This result is in general agreement with recent observations by Van der Haar and Hanson (1969), Van der Haar and Oort (1973) and Raschke et al (1973). However, the major climatological discrepancies resulting from the specification of layered cloud amounts in the tropics in a manner identical to that used poleward of the subtropics still seems to give somewhat excessive albedo. It is felt that the geometry of solar radiation streams impinging upon subgrid sized cumulus cells in the tropics should be remodeled so as to divert a greater percentage of solar radiation downward, as compared with the characteristic cloud-layering and resultant reflective effects which seems permissible in middle and high latitudes.

II. DATA PREPARATION

A. INITIAL DATA FIELDS

The temperature and humidity data used in this study were arranged in the form of soundings taken along four oceanic meridians (Fig. 1) of the Fleet Numerical Weather Central (FNWC) Northern Hemisphere analyses on 16 April 1974. Computation of radiational dispositions and of other heat budget terms are made at these gridpoints. Oceanic locations for these computations were chosen because:

1. The constant σ surfaces (where $\sigma = \frac{P}{\pi}$) of the FNWC primitive equation system are close to being constant pressure levels.

2. The maritime-area heating rate computations are likely to be representative of the month of April 1974 as contrasted with computations made for 16 April 1974 over a corresponding set of gridpoints over land.

The three meridians (and their respective number of soundings) selected over the Pacific Ocean were located at 125W (25 soundings), 170W (25 soundings) and 145E (17 soundings). The Atlantic Ocean meridian was 35W (26 soundings). This method of selecting "soundings" along the indicated meridians of the FNWC polar stereographic map, made it unnecessary to employ spatial interpolation between original data gridpoints along the meridians. Data along line 3 in the Pacific was

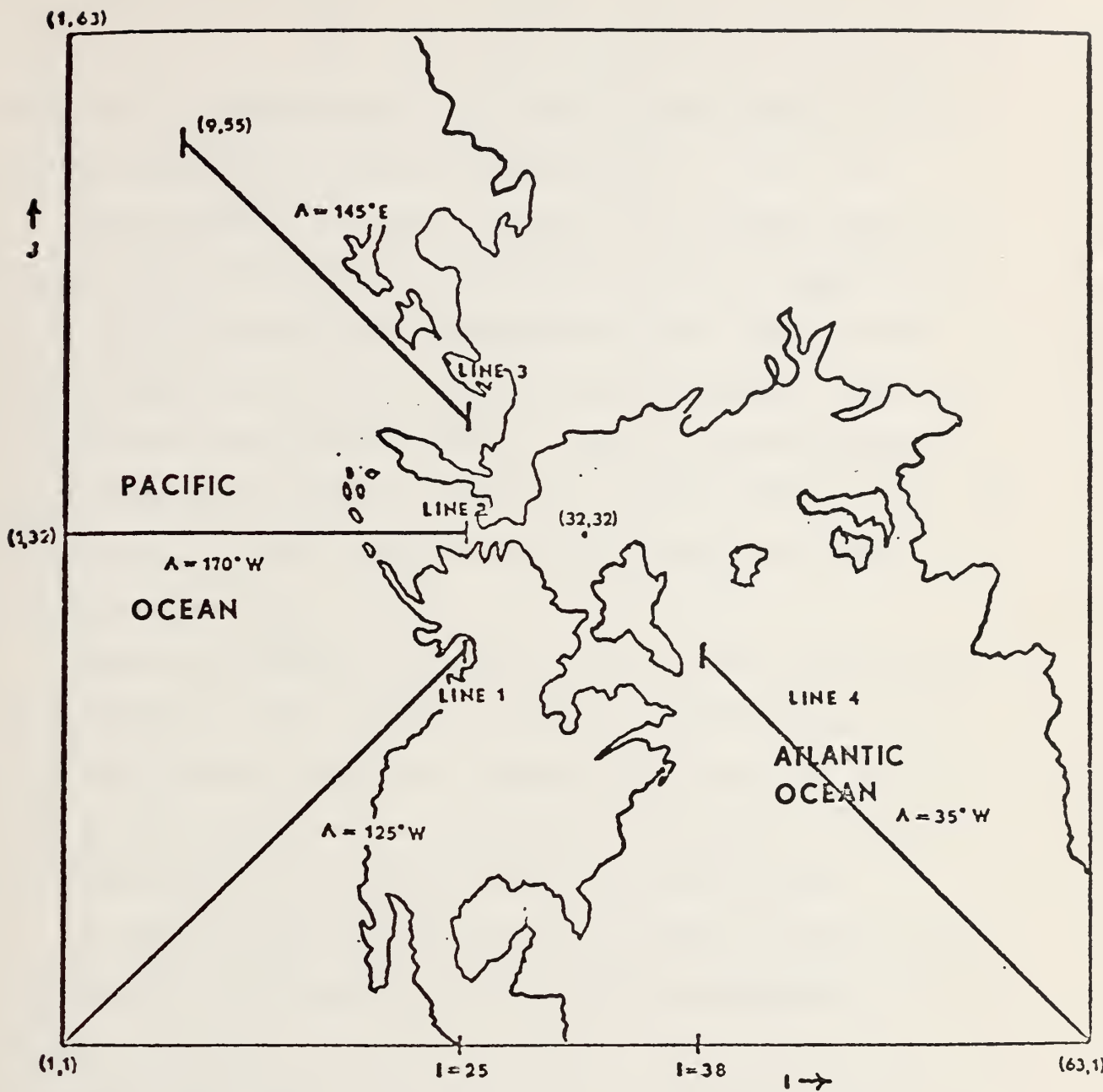


Figure 1. FNWC polar stereographic grid and meridians (lines 1, 2, 3, and 4) selected for study. The longitudes Λ are shown for each meridian as well as the extent considered of each meridian.

not extended southward of gridpoint (9,55) because they fell over land masses (New Guinea and Northern Australia) where the surface temperatures and other sounding features were unrepresentative of the oceanic values.

The gridpoint soundings in the form of Table I(a) were taken from the original FNWC 63-by-63 surface analysis, as well as of the vertical distribution of T(P) and of dew point depression at five other standard pressure levels up to and including 400 millibars. These original soundings were then modeled into a radiative sounding (Table I(b)) corresponding to FNWC primitive equation prediction levels up to 100 mb (see Fig. 2).

Data from 0000GMT, 16 April 1974 were used for the Pacific soundings while 1200GMT, 16 April 1974 data were used for the Atlantic soundings. These times were used so that the analysis times would correspond as closely as possible to local solar noon in each of the indicated areas.

At each gridpoint selected, the original humidity data was given in the form of five dew point depressions for the analysis levels from 925mb to 400mb. Since the standard instrument level vapor pressure (e_{air}) was missing from the original FNWC analysis at all gridpoints, e_{air} was approximated using the FNWC field of e_x , a computed value of vapor pressure at about 20 meters above mean sea level (MSL) in the turbulent boundary layer. FNWC values of T_x and e_x over the ocean had been made available using an operational planetary boundary layer model detailed by Kaitala (1974).

Table I(a). Example of typical FNWC sounding for gridpoint (1,1). The humidity parameters between 925,..., 400mb are dew point depressions, but at the surface and top of the constant flux layer (9999*) are vapor pressures in mb.

Pressure (mb)	T (°C)	Humidity Parameters
Surface, 1000 mb	25.6	$e_x = 27.4$ mb
925	18.3	1.2 C
850	14.6	1.0 C
700	5.6	3.4 C
500	-11.0	2.8 C
400	-22.7	1.4 C
300	-37.6	
250	-46.5	
200	-56.3	
150	-67.3	
100	-80.6	
9999*	Tx = 23.5	

* Code 9999 indicates data taken from the top of the constant flux level (CFL) of the FNWC initial data program.

Table I(b). Example of the corresponding radiative sounding with mixing ratio listed at odd k-levels (Fig. 2). Additionally, water vapor and CO₂ absorber masses, cloud amounts, CL(1) and CL(2) (after Smagorinsky (1960)) as these parameters are modeled in the radiative theory.

Pressure (mb)	T(°C)	Mixing Ratio g/kg	Absorber Masses		Smagorinsky Cloud Amounts	
			water vapor (gm/cm ²)	CO ₂ (cm/cm ²)	CL(1)	CL(2)
1000	25.60	17.10				
900	16.67	12.56				1.000, CL ₂
800	11.84		2.35	45.53		
700	5.60	6.43				
600	-1.57		3.36	83.53		
500	-11.00	2.68				0.900, CL ₁
400	-22.70	1.41	3.69	113.35		
300	-37.60	0.68				
200	-56.30		3.75	133.99		
100	-80.60	0.04	3.75	138.67		
0	-80.60	.00	3.75	143.35		

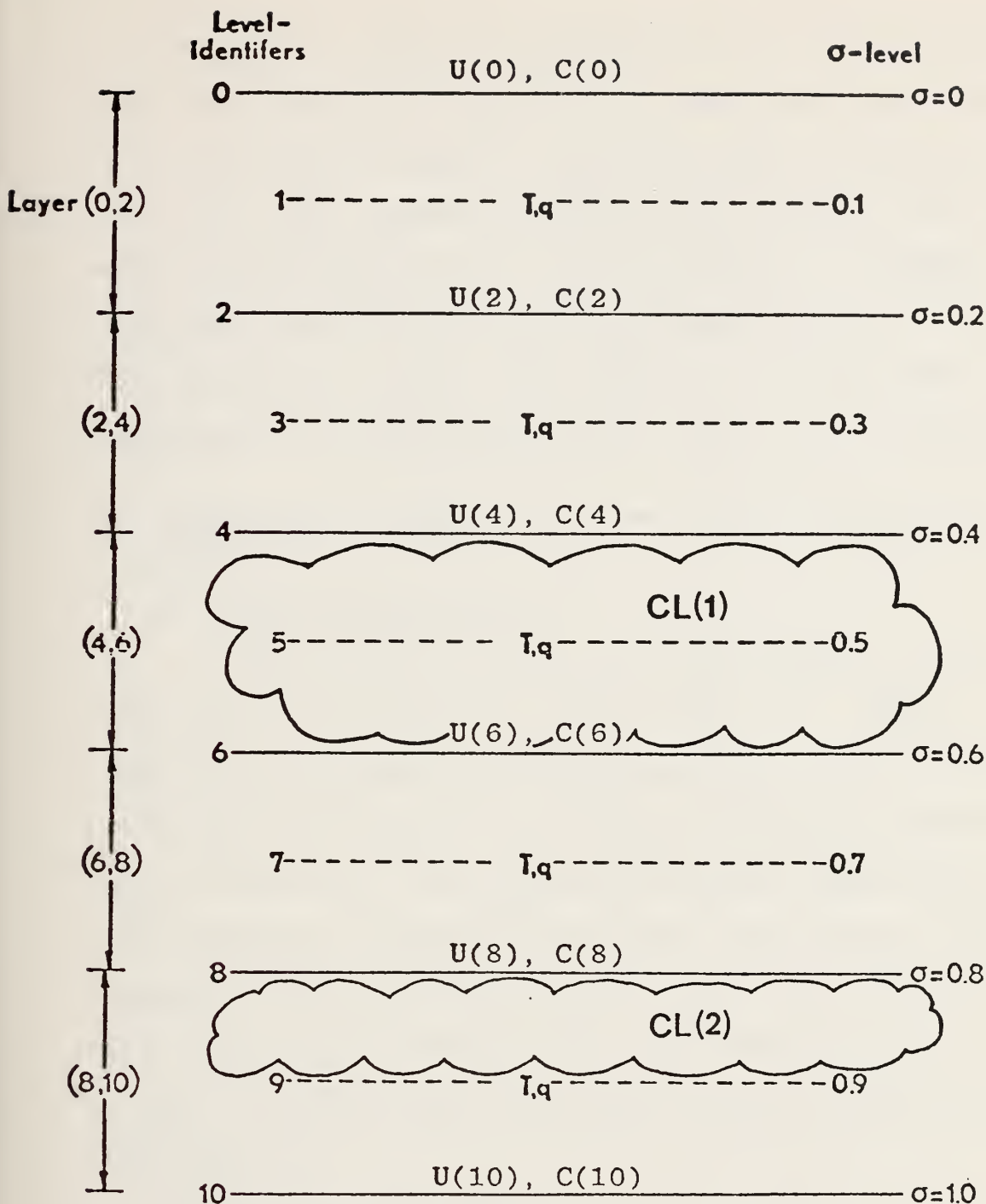


Figure 2. Five-layer radiative sounding used in this study. Levels are identified by their values on the k-scale, while layers are identified by their level boundary indicies in parentheses, e.g. (8,10). Pressure-scaled water vapor and CO_2 mass increments ΔU and ΔC , respectively are integrated relative to the surface and the resulting U and C are carried in the model at even levels. The temperature T is retained at all levels. Amounts of clouds CL(1) and CL(2) in the layers shown have been parameterized for consideration of their radiative effects.

To perform radiative calculations, it is necessary to have water vapor and CO_2 absorber masses and cloud amounts, CL(1) and CL(2) at certain required k-level boundaries (Fig. 2). All soundings in this study start at sea level with the approximation of surface pressure $\pi \doteq 1000\text{mb}$. Therefore, the k-levels correspond approximately to the FNWC levels $P_k = 1000., 900., 800., \dots, 200., 100., 0.0\text{mb}$ corresponding respectively to $\sigma_k = 1.0, 0.9, \dots, 0.1, 0.0$.

B. INTERPOLATIVE PROCESSING TO k-LEVELS IN RADIATIVE SOUNDINGS

1. Temperature Profiles

The gridpoint temperatures were listed at each mandatory level of Table I(a) between 1000., ..., 100mb. The temperature was assumed to be isothermal from 100mb to $p=0.0\text{mb}$. The temperature T_{10} was set equal to the FNWC listed sea-surface temperature. The radiative sounding temperatures for the remaining k-levels were obtained from either their corresponding listed temperature-level or by a three-point Lagrangian interpolation scheme (Eq. 2-1, Spaeth, 1975), to level k when the listed FNWC temperature-profile did not include the value T_k .

2. Moisture Profiles

The moisture from the original FNWC soundings (Table I(a)) were converted into mixing ratios at each of the original sounding levels. The near-surface vapor pressure (taken as e_x) was used to calculate the mixing ratio at $k=10$

as described by Spaeth (1975):

$$q_{10} = 621.97 (e_x/1000) \quad (2-1)$$

The remaining ratios q were calculated from the original FNWC sounding (Table I(a)) dew point depression data after Spaeth (1975, Eq. 2-3). The computed q -values were subsequently interpolated to k -levels using the previously mentioned three-point Lagrangian procedure applied to successive q -values in the original sounding. Resulting values of the interpolated q -values are shown for the case of the radiative sounding at gridpoint (1,1) (Table I(b)).

Due to the fact that most radiosonde humidity data for $p \leq 300\text{mb}$ is either unreliable or not available, a power-law extrapolation formula (Spaeth, 1975)

$$\frac{q_k}{q_5} = \left(\frac{P_k}{500}\right)^\lambda \quad (2-2)$$

was used to obtain q -values at $k=3,2,1$.

This extrapolative procedure for obtaining q -values at high levels was first suggested by Smith (1966), utilizing the least squares estimation of λ according to

$$\lambda = \frac{\sum_{i=1}^6 y_i x_i}{\sum_i x_i^2} = R_{yx} \sqrt{\frac{\sum y_i^2}{\sum x_i^2}} \quad (2-3)$$

with $y_i = \log \frac{q_i}{q_5}$ and $x_i = \log(P_i/P_5)$. The Smith method was then further tested by Spaeth (1975) for the vertical scale

of the FNWC initial data soundings. The resulting correlation coefficient R_{yx} was generally found to lie in the range .95 to .99. Such high correlations indicate that the procedure described by Spaeth (1975) for determining upper atmosphere q-values has realistic estimation value for the vertical scale involved in the radiative sounding.

3. Pressure-Scaled Absorber Masses

The pressure-scaled water vapor absorber mass Δu in a layer (Fig. 2) was calculated for the five odd numbered k-levels by using the computed mixing ratio values (Eq. 2-7, Spaeth, (1975)). The equation for computing the integrated pressure-scaled water vapor mass is given by the algorithm described by Eq. 2-8 of Spaeth.

A similar algorithm was used in the computation of the carbon-dioxide scaled absorber mass (Spaeth, 1975, Eq. 2-10,11). To be noted here is the fact that CO_2 absorber masses have been stated in terms of N.T.P. "pressure-scaled" cms, since the CO_2 absorption coefficients are generally stated in terms of this CO_2 mass unit.

C. CLOUD PARAMETERIZATION

The relative humidities, and thus the saturation vapor pressure at levels $k=5$ and $k=9$, are used in the calculations of the fractional cloud cover CL_1 and CL_2 in layers (4,6) and (8,9) respectively, as depicted in Fig. 2. The fractional

cloud amounts for these two layers were parameterized using the following equations (after Smagorinsky, 1960):

$$CL(1) = 2.0 (RH(5)) - 0.7 \quad (2-4(a))$$

$$CL(2) = 3.33(RH(9)) - 2.0 \quad (2-4(b))$$

Smagorinsky's parameterization of CL(1) and CL(2) permits cloudiness fractions of 1.30 and 1.333 respectively with RH=1.0. Values of CL greater than 1.0 were considered initially by Smagorinsky (1960) to suggest the amount of supersaturation which accompanies precipitation.

All operational radiative models in use at the present time limit $CL \leq 1.0$. In the radiative study developed here no opportunity is afforded to deduce precipitation-rates and/or supersaturation amounts. Hence, the Smagorinsky formulations of CL_1 and CL_2 were reduced in each case by the multiplicative factor 2/3 so that neither fractional cloud cover could exceed unity. Thus alternative cloud-cover fractions

$$CL'_1 = 2/3 (CL_1) \quad (2-5(a))$$

$$CL'_2 = 2/3 (CL_2) \quad (2-5(b))$$

were considered for purposes of estimating the shift in the global radiative balance as a result of altering the cloud computations in the radiation model.

The 1/3 reduction inherent in CL'_1 , CL'_2 relative to Smagorinsky's CL_1 , CL_2 were initiated in this study in an

attempt to tune cloud amounts to give radiation results in closer agreement with recent satellite climatology of Raschke et al, (1973). This satellite climatology suggests the use of smaller cloud amounts than that specified by Smagorinsky. Fractional cloud amounts were considered to be functions of large scale effects only. Therefore, small scale convective activity, seasonal conditions (except for the soundings) and latitudinal effects were not considered in specifying the reduction factor of Eq. 2-5. The reduced cloud-parameterization was introduced here for estimating large scale radiational effects only.

D. CLOUD-AREA COVERAGES

Since Eqs. 2-4a,b or 2-5a,b gave the fractional-coverage of the gridpoint area by the appropriate cloud-type, the gridpoint area may be thought of as broken into random fractional segments of size

$$W(0,0) = (1-CL_1) (1-CL_2) \quad (2-6a)$$

wherein there is a combination of clear-over-clear segments in the layers. Similarly, the gridpoint area has the fractional area of cloud coverage

$$W(1,1) = CL_1 * CL_2 \quad (2-6b)$$

of upper-cloud amount CL_2 overlying lower-cloud amount CL_2 . Likewise the combinations of cloudy over clear and clear

over cloudy , by layers, may be visualized as occurring with the respective weights

$$W(1,0) = CL_1 * (1-CL_2) \quad (2-6c)$$

and

$$W(0,1) = (1-CL_1) * CL_2 \quad (2-6d)$$

Regardless of whether the full-cloud amounts CL_1 , CL_2 of Smagorinsky (Eq. 2-4), or the 2/3-CL amounts of Eq. 2-5 were utilized, it was useful to carry, for radiation computations of each sounding, the relative weights or fractions of the gridpoint area exposed to the specified cloud-layer combinations. Henceforth, the symbols denoted by $W(0,0)$, $W(1,1)$, $W(1,0)$, $W(0,1)$ and as given by Eqs. 2-6(a,b,c,d), suggest overcast (1) or clear (0) cloud amounts in the indicated layers (Fig. 2), the first index 1 or 0 referring to layer CL_1 , and the second to CL_2 .

The usefulness of this computational device will be clarified in Sections III and IV, where the procedures for the terrestrial and solar radiational computations are discussed and the results are summarized over the set of soundings.

III. TERRESTRIAL RADIATION

A. THEORETICAL AND EMPIRICAL BASIS

Empirical formulas were developed by Sasamori (1968) for flux emissivities in the atmosphere associated with computations for the heat balance requirements of the NCAR General Circulation Model. Sasamori derived the empirical emissivity formulas for water vapor and CO_2 by comparison with the theoretical values built into the Yamamoto Radiation Chart (1952). This chart has proved to be quite accurate for computational checking of the Sasamori emissivities and was used by Spaeth (1975) and Warner (1974) as a systematic guide for integration of the radiative transfer formulas developed by Martin (1972, 1974), who adapted the Sasamori formulas to the particular layers of interest in the gridpoint computations of the FNWC primitive equation model (Fig. 2).

The essential long-wave flux formulas required for use in the FNWC heating package are the following:

$$F_{10}^* = \text{net IR flux at earth, } k=10$$

$$F_6^* = \text{net IR flux at level } k=6$$

$$F_2^* = \text{net IR flux at level } k=2$$

$$F_{610} = \text{net IR flux divergence in the layer } (6,10)$$

$$F_{26} = \text{net IR flux divergence in the layer } (2,6)$$

To get the IR flux divergences in the layers (6,10) and (2,6), the differences $F_6^* - F_{10}^*$ and $F_2^* - F_6^*$ must be computed.

The detailed scheme for making such computations with various combinations of cloud cover CL(1) and CL(2) is similar to the technique developed by Martin (1974) and as reproduced in detail by Spaeth (1975).

In order to make IR net-flux calculations along the path of integration, there must be a physically sound representation of the emissivity (ϵ_{wc}) as a function of both water vapor and CO₂ absorber masses in layers along the sounding. For a further discussion of the emissivity formulas used in the quadrature scheme, refer to Spaeth's Appendix A (1975).

B. NET FLUX FORMULATION

1. At Level k=10

The radiative sounding as depicted in Table I(b), was computed as the combination of parameters U(k,10), C(k,10) and T_k for each required level, k=10,8,...,2,1,0. Cloud parameters CL(1) and CL(2) are also listed at each gridpoint and in general are non-zero. The grid area was then considered to be composed of areal fractions (weights) defined in Eqs. 2-6(a,...,d) and denoted by the symbols W(0,0), W(1,1), W(1,0), W(0,1).

The composite net flux F_{10}^* (CL₁, CL₂) at level k=10 at each gridpoint is then constructed by using the appropriate weight factor to multiply the reference net flux F_{10}^* computations defined for the special cloud-cover cases

$$F_{10}^*(0,0), F_{10}^*(1,0), F_{10}^*(0,1), F_{10}^*(1,1)$$

so that

$$F_{10}^*(CL_1, CL_2) = W(0,0)F_{10}^*(0,0) + W(1,0)F_{10}^*(1,0) \\ + W(0,1)F_{10}^*(0,1) + W(1,1)F_{10}^*(1,1) \quad (3-1)$$

Spaeth (1975) has listed these reference net flux formulations in his Eqs. 3-6, 7,8. Using the definitions of $W(0,0)$, $W(1,0)$, $W(0,1)$, $W(1,1)$, $F_{10}^*(CL_1, CL_2)$ can be shown to assume the form

$$F_{10}^*(CL_1, CL_2) = [1-CL(2)]\{(B_{10}-B_6) - .5[\epsilon_{wc}(8,10)(B_{10}-B_8) \\ + (\epsilon_{wc}(8,10) + \epsilon_{wc}(6,10))(B_8-B_6)]\} \\ + (1-CL(2))(1-CL(1))\{B_6 - .5[(\epsilon_{wc}(6,10) \\ + \epsilon_{wc}(4,10))(B_6-B_4) + (\epsilon_{wc}(4,10) \\ + \epsilon_{wc}(2,10))(B_4-B_2) + (\epsilon_{wc}(2,10) \\ + \epsilon_{wc}(1,0))(B_2-B_1) + \tilde{\epsilon}_{wc}((0,10), T_1)*B_1]\} \\ + CL(2)\{(B_{10}-B_9)[1-.5\epsilon_{wc}(9,10)]\} . \quad (3-2)$$

Here

$$B_k = 1.170403 \times 10^{-7} T_k^4 \quad (3-3)$$

is the Stefan-Boltzmann blackbody flux in langlies per day.

Further, $\epsilon_{wc}(U_k, C_k, 10)$ is the combined water-vapor and CO_2 emissivity along the path from level 10 to level k. This emissivity is considered by Sasamori to be temperature independent for $T \geq 210K$, whereas $\tilde{\epsilon}_{wc}$ represents the

temperature dependent emissivity applicable for $T < 210K$ (see pp. 136-137, Spaeth, 1975).

The reference net fluxes F_{10}^* of Eq. 3-1 are associated with (1) clear skies in both layers, (2) overcast in the upper layer only, (3) overcast in the lower layer only and (4) overcast in both layers respectively.

2. Net Flux F_6^*

The formula for $F_6^*(CL_1, CL_2)$ has been developed by Spaeth (Eq. 3-10, 1975) in a manner analogous to the derivation of the weighted F_{10}^* . The result is reproduced after Spaeth (1975, see pp. 43).

$$\begin{aligned}
 F_6^* = & [1-CL(1)]\{B_8-.5[\epsilon_{wc}(6,8)(B_8-B_6)+\epsilon_{wc}(4,6)(B_6-B_4) \\
 & +(\epsilon_{wc}(4,6)+\epsilon_{wc}(2,6))(B_4-B_2)+(\epsilon_{wc}(2,6) \\
 & +\epsilon_{wc}(1,6))(B_2-B_1)+\tilde{\epsilon}_{wc}((0,6),T_1)*B_1]\} \\
 & +(1-CL(1))(1-CL(2))\{(B_{10}-B_8)[1-.5(\epsilon_{wc}(6,8) \\
 & +\epsilon_{wc}(6,10))]\}+CL(1)\{(B_8-B_6)^* \\
 & [1-.5\epsilon_{wc}(6,8)]\}+CL(1)(1-CL(2))\{(B_{10}-B_8)^* \\
 & [1-.5\epsilon_{wc}(6,8)+\epsilon_{wc}(6,10))]\} .
 \end{aligned} \tag{3-4}$$

3. Net Flux F_2^*

The net flux at level $k=2$ can be calculated in a similar fashion to F_{10}^* and F_6^* , with the formulation of the individual reference net fluxes F_2^* as previously described.

The formula for $F_2^*(CL_1, CL_2)$ is then developed analogous to that for $F_{10}^*(CL_1, CL_2)$ and $F_6^*(CL_1, CL_2)$.

$$\begin{aligned}
 F_2^* = & [1-CL(1)]\{B_8-.5[\epsilon_{wc}(2,4)(B_4-B_2)+(\epsilon_{wc}(2,4) \\
 & + \epsilon_{wc}(2,6))(B_6-B_4)+(\epsilon_{wc}(2,6)+\epsilon_{wc}(2,8))* \\
 & (B_8-B_6)+\epsilon_{wc}(1,2)(B_2-B_1)+\tilde{\epsilon}_{wc}((0,2),T_1)*B_1]\} \quad (3-5) \\
 & +(1-CL(1))(1-CL(2))*\{(B_{10}-B_8)[1-.5(\epsilon_{wc}(2,8) \\
 & + \epsilon_{wc}(2,10))]\}+CL(1)\{B_4-.5[\epsilon_{wc}(2,4)(B_4-B_2) \\
 & + \epsilon_{wc}(1,2)(B_2-B_1)+\tilde{\epsilon}_{wc}((0,2),T_1)*B_1]\} .
 \end{aligned}$$

A new parameter, the total outgoing long-wave radiation to space (FF2) can be readily defined from the expression for F_2^* by setting to zero the terms of Eq. 3-5 representing the downward flux through level $k=2$. These terms are just those denoted by the symbols $\tilde{\epsilon}_{wc}((0,2),T_1)*B_1$ and $\epsilon_{wc}(1,2)(B_2-B_1)$. If the long-wave radiative model, including its cloud parameterization, is realistic, the modeled outgoing flux to space (FF2) should compare reasonably with that observed by NIMBUS III satellite during the same period, after Raschke et al (1973). The most nearly comparable satellite climatological period was 1-15 May 1969. These satellite observations were obtained from the NIMBUS III satellite atlas of Raschke et al (1973) for the May dates indicated and used for comparison with the model values of FF2, point for point (at 5°latitude intervals) along the

same four meridians of Fig. 1. Also the latitudinally-distributed mean satellite fluxes were compared with the corresponding averaged values of FF2. The results showing the comparisons of the model computations of FF2 with the corresponding satellite observations are listed by latitude in Table V.

C. APPLICATIONS TO HEAT BALANCE COMPUTATIONS

1. At Upper and Lower Boundaries

In order to compute the heat balance at the top of the earth-tropospheric system the composite F_2^* and the total insolation absorbed below level $k=2$ at each gridpoint are required. Moreover a radiative balance is computed at the surface for each gridpoint using the earth's absorbed insolation (Section IV) and the composite net flux loss F_{10}^* .

In order to consider the possibility of a heat balance at the earth's surface, rather than merely a radiative balance, it is necessary to add a term representing combined sensible and latent heat transfer across the air-sea interface (Section V). This latter transfer rate at each gridpoint was adapted from the FNWC primitive equation model, after the discussion of Kaitala (1974) and based upon the FNWC data of 16 April 1974.

2. Intermediate Levels

Consideration of the radiation balance in the atmosphere requires computation of the long-wave cooling effects

caused by the flux divergences F26 and F610. F26 and F610 are defined as

$$F26 = F_2^* - F_6^* \quad (3-6)$$

$$F610 = F_6^* - F_{10}^* \quad (3-7)$$

where the symbols (2,6) and (6,10) indicate the layer boundaries involved in the balance considerations for the indicated layer.

In order to compute F26 and F610 at each gridpoint, complete listings of IR net fluxes F_{10}^* , F_6^* , F_2^* , associated with each set of reference cloud amounts (0,0), (1,0), (0,1), (1,1) have been computed at each gridpoint together with the weighted set of fluxes $F_{10}^*(CL_1, CL_2)$, $F_6^*(CL_1, CL_2)$, $F_2^*(CL_1, CL_2)$. These cloud-weighted values have been constructed using the weighting scheme of Eqs. 2-6, 3-1, 3-4 and 3-5. A sample gridpoint printout of the net fluxes has been included in Table II.

The determination of the heat balance by layers has been deferred to Section VI, where the results are displayed in cross-sectional form for the 2/3-CL case.

D. STATISTICAL RESULTS AND COMPARISONS

1. Net Flux $F_{10}^*(0,0)$

A statistical test of the $F_{10}^*(0,0)$ numerical results was conducted by utilizing a linear regression program for relating the predictand $F_{10}^*(0,0)$ against the simultaneous values of $X_1=B_{10}$ and $X_2=B_{10}\sqrt{e}$ as predictors, using all 93

gridpoint data as samples. The regression program was based on the BMD02R in the Biomedical set of programs (Dixon, 1973). The result was cast in the form of the well-known Brunt net flux equation (1932):

$$F_{10}^* = B_{10}(a + b\sqrt{e}) \quad (3-9)$$

where

$$B_{10} = St * T_{10}^4$$

is the Stefan-Boltzmann blackbody flux at the surface temperature T_{10} and e is the surface vapor pressure in mb. The multiple correlation coefficient $R_M(F_{10}^* | X_1, X_2)$ was higher than 0.99 in the 16 April case, as was also true for the data periods of Spaeth (16 January 1974), and Beahan (16 July 1974), (Table III).

Since F_{10}^* may be defined as

$$F_{10}^* = B_{10} - F_d \quad (3-10)$$

Eq. 3-10 can then be solved for F_d

$$F_d = B_{10}\{(1-a)-b\sqrt{e}\} , \quad (3-11)$$

for the clear-sky case. It must be recalled that the computation of F_d included both the effects of water-vapor and of CO_2 . Since there is no direct relationship of \sqrt{e} upon the quasi-constant absorber mass of CO_2 , the radiative effect of the latter constituent in Eq. 3-10 must be included in the term involving $(1-a) B_{10}$.

CL(1) = 0.0	CL(2) = 0.0	WT = 0.0	$F_{10}^* = .1635$	$F_6^* = .2645$	$F_2^* = .3483$	ly/min
CL(1) = 1.0	CL(2) = 0.0	WT = 0.0	$F_{10}^* = .0912$	$F_6^* = .0907$	$F_2^* = .2347$	ly/min
CL(1) = 0.0	CL(2) = 1.0	WT = .1000	$F_{10}^* = .0481$	$F_6^* = .2352$	$F_2^* = .3212$	ly/min
CL(1) = 1.0	CL(2) = 1.0	WT = .9000	$F_{10}^* = .0432$	$F_6^* = .0614$	$F_2^* = .2347$	ly/min
COMPOSITE TOTALS						
			$F_{10}^* = .0432$	$F_6^* = .0787$	$F_2^* = .2434$	ly/min

Table II. A sample listing of gridpoint values of the terrestrial radiation fluxes computed at gridpoint (1,1) using the equations detailed in Sec. III.

A cross-seasonal comparison of the coefficients $1-a$ and $-b$ of Eq. 3-11 is presented in Table III, comparing the clear-sky results of F_d for 16 April 1974 with those of Spaeth and Beahan at intervals of three months earlier and later, respectively.

The high multiple correlation coefficients indicate that an oceanic version of the Brunt downward flux equation is valid for each tested season. F_d depends most strongly upon B_{10} while only slightly on $B_{10}\sqrt{e}$. This is an apparent result of the nearly constant relative humidity over the large oceanic regimes. Moreover, the weak dependence of F_d upon $B_{10}\sqrt{e}$ is most evident at the data-time 16 July 1974, when the coefficient $-b$ is smallest. This characteristic is due primarily to the relatively weak gradient of \sqrt{e} in the radiative soundings aloft.

	<u>16 January 1974</u>	<u>16 April 1974</u>	<u>16 July 1974</u>
$1-a$.6436	.6557	.8129
$-b$.0224	.0209	-.0094
$\overline{F_d}$.4500	.4527	.5471
R_M	.9955	.9969	.9950

Table III. Cross-seasonal comparisons of the coefficients $1-a$ and $-b$ from Eq. 3-11. The mean values F_d from the Brunt equation and the resulting multiple correlation coefficients have been included.

2. Modification of F_{10}^* for Cloudiness CL_1, CL_2

A second statistical test was performed based on a possible relationship between the cloudy-sky and the clear-sky

cases of F_{10}^* . The ratio $Y = F_{10}^*(CL_1, CL_2)/F_{10}^*(0,0)$ was used as the predictand in this case. The predictor CL was the total opaque cloud cover at each gridpoint, defined as (after Quinn, 1971 and Spaeth, 1975):

$$CL = CL(1) + CL(2) (1-CL(1)) . \quad (3-12)$$

This regression was developed utilizing $F_{10}^*(CL_1, CL_2)$ in the numerator, computed with the amounts CL(1) and CL(2) as calculated from Smagorinsky's formulation, and then utilizing $F_{10}^*(CL'_1, CL'_2)$ computed from the 2/3-CL parameterization. The general form of the regression formula required is shown in Eq. 3-13 below, with CL given by Eq. 3-12 above.

$$F_{10}^*(CL) = F_{10}^*(0,0) [1-d(CL)] . \quad (3-13)$$

A cross-seasonal comparison of the coefficients d and other statistics for the 2/3-CL and full-CL cases using the results of this study and those of Spaeth and Beahan, is presented in Table IV. There seems to be little clear-cut variation in the statistics of Table IV between the results of adjacent seasons, and little statistical preference between the full-CL and the 2/3-CL cases.

The high correlation coefficients of Table IV for all seasons considered, indicate the general capability of the IR radiative model employed in this study to account for the effective net radiation at the surface.

	16 January 1974		16 April 1974		16 July 1974	
	2/3-CL	Full-CL	2/3-CL	Full-CL	2/3-CL	Full-CL
d	.75	.75	.73	.75	.79	.81
R _M	.9936	.9916	.9945	.9942	.9920	.9916

Table IV. Cross-seasonal comparison of the coefficient d from Eq. 3-13 and the resulting multiple correlation coefficients for both the 2/3-CL and the full-CL cases.

The mean values of F_{10}^* over the 93 gridpoint soundings for 16 April 1974, as applicable in Tables III and IV were as follows:

Full-CL Statistics	2/3-CL Statistics
$\overline{F_{10}^*(CL)} = .0639 \text{ ly min}^{-1}$	$\overline{F_{10}^*(CL)} = .0868 \text{ ly min}^{-1}$
$\overline{F_{10}^*(0,0)} = .1515 \text{ ly min}^{-1}$	$\overline{F_{10}^*(0,0)} = .1515 \text{ ly min}^{-1}$
$\overline{CL} = .7733$	$\overline{CL} = .5888$

The superior bar symbol denotes the sample mean. These results indicate that the surface net flux is decreased by the respective ratios .578 with $\overline{CL} = .7733$, and by .427 with $\overline{CL} = .5888$. These results indicate that the downward flux $\overline{F_d(CL)}$ is 57.8 percent larger at the surface than $\overline{F_d(0,0)}$ when full-CL amounts are used in the cloud parameterization model. In the 2/3-CL parameterization the mean downward flux at the surface $\overline{F_d(CL')}$ is increased by only 42.7 percent when compared to $\overline{F_d(0,0)}$.

E. COMPARISONS OF FF2 WITH SATELLITE CLIMATOLOGY

Comparison was made of computed-model values of FF2 with satellite measurements of total long-wave flux to space

(after Raschke et al, 1973) for the NIMBUS III period of 1-15 May 1969. FF2 is used here instead of F_2^* since the downward flux at $k=2$ is not measured by the satellite. The computation of FF2 was previously discussed. FF2 for 16 April 1974 was computed for both full-cloud and 2/3-CL cases at all 93 gridpoints. These FF2 values were then interpolated to whole multiples of 5 degrees of latitude along each of the four meridians and the results were then averaged to get a mean latitudinal distribution value for each 5 degree latitude interval considered in this study.

Table V shows both of the latitudinally distributed FF2 cloud-model values compared with those extracted from Raschke et al (1973). Raschke's results were obtained by interpolation from charts using the same oceanic meridians as those used in this study. Latitudinally distributed total opaque cloud cover CL by Eq. 3-12 are also listed for both the full and 2/3-CL cases at each latitude. In the bottom line of each column in Table V is listed the cosine weighted mean of each set of the column values for the listed latitude range (see Eq. 7-2 for the equation defining "weighted average").

It should be noted that the Raschke results do not correspond to specifically known CL values. Both cloud cases give FF2 results which are reasonably close to the values reported by Raschke, especially the means and between 5N-25N. Neither the full-CL nor the 2/3-CL model can be conclusively selected as preferable, based on Table V results alone. The limitations

of the comparisons made here are obvious, when it is recalled that between latitudes 20S-5S and between 60N-65N there are fewer than four meridional lines available for computing the listed zonal values in Table V. For all other latitudinal average values, four meridional lines were used in the averaging.

F. COMPARISONS OF CROSS-SEASONAL RESULTS OF F_{10}^*

Table VI depicts the latitudinally-distributed values of F_{10}^* and of CL at the earth's surface obtained using the 2/3-CL parameterization. A seasonal comparison of the model computed F_{10}^* is made with data obtained from Spaeth (1975) for the 16 January 1974 and from Beahan (1975) for 16 July 1974 cases. It is clearly shown that $F_{10}^*(CL')$ is a decreasing function of cloud cover. There is a clear-cut tendency in each season for a maximum value of F_{10}^* to be located in the subtropics (latitudes 15N-25N). Also there is evidence of a high latitude (55N-60N) minimum F_{10}^* associated with a concentration of maximum cloud cover CL' . The most outstanding variation is the transition in the Southern Hemisphere latitudes (20S-10S), which has large cloud cover in both the January-April monsoon period but only small CL' in the July data period. The same relative conclusions resulted when the full-CL parameterization was examined for cross-season comparisons, but the obtained results are not included in Table VI.

Lat.	FF2		F2(RAS) (Raschke)	Cloud-Amounts	
	(Full-CL)	(2/3-CL)		Full-CL	2/3-CL
20S	.2581	.2852	.41	.985	.842
15	.2688	.2942	.42	.983	.828
10	.3005	.3203	.41	.944	.752
5	.3220	.3383	.40	.842	.647
0	.3216	.3381	.37	.878	.659
5	.3499	.3614	.35	.829	.591
10	.3711	.3801	.37	.823	.639
15	.3714	.3804	.39	.799	.548
20	.3752	.3815	.39	.788	.536
25	.3768	.3817	.39	.642	.473
30	.3463	.3539	.38	.582	.446
35	.3290	.3373	.36	.634	.520
40	.3099	.3206	.33	.630	.468
45	.2914	.3011	.34	.630	.467
50	.2763	.2893	.34	.877	.674
55	.2665	.2793	.37	.719	.555
60	.2369	.2530	.31	.962	.816
65N	.1815	.2085	.30	.985	.796
<hr/>					
Wt avg	.3264	.3383	.3740	.796	.596

Table V. Comparison of zonally averaged longwave flux to space, FF2, as found by this study for both full-CL and 2/3-CL cloud cases for 16 April 1974, and F2(RAS) by Raschke et al (1973) based upon NIMBUS III measurements. Also included are composite cloud-amount fractions used in the two cloud models of this study. Flux values in ly min^{-1} .

Lat	16 January 1974		16 April 1974		16 July 1974	
	$F_{10}^* (\frac{2}{3} - CL)$	$\frac{2}{3} - CL$	$F_{10}^* (\frac{2}{3} - CL)$	$\frac{2}{3} - CL$	$F_{10}^* (\frac{2}{3} - CL)$	$\frac{2}{3} - CL$
20S	.078	.758	.074	.842	.151	.269
15	.079	.733	.067	.828	.133	.306
10	.086	.634	.071	.752	.135	.258
5	.090	.536	.081	.647	.093	.498
0	.082	.556	.073	.659	.100	.445
5	.086	.527	.080	.591	.095	.534
10	.107	.376	.086	.639	.102	.460
15	.115	.342	.092	.548	.103	.430
20	.120	.279	.085	.536	.094	.431
25	.120	.320	.094	.473	.098	.375
30	.111	.411	.098	.446	.092	.425
35	.122	.382	.112	.520	.092	.383
40	.108	.529	.116	.468	.085	.387
45	.067	.740	.100	.467	.071	.566
50	.069	.759	.080	.674	.064	.475
55	.068	.749	.108	.555	.038	.819
60	.106	.538	.054	.816	.085	.459
65N	.095	0.0	.082	.796	.061	.590
Wt Avg	.096	.514	.086	.596	.092	.405

Table VI. Cross-seasonal comparison of the zonally-averaged net fluxes at the surface F_{10}^* , and cloud coverage based on 2/3-CL parameterization for the six-month interval of 16 January 1974 to 16 July 1974. Flux values in $ly\ min^{-1}$.

IV. SOLAR RADIATION

A. PARTITION OF SOLAR INSOLATION

The solar constant assumed in this study at level $k=0$ (top of atmosphere) was 2.00 ly min^{-1} (Joseph, 1971). This flux was depleted by 4% to account for the attenuation caused by oxygen and ozone above the tropopause. This left the value $S = 1.92 \text{ ly min}^{-1}$ at level $k=2$ to be used in this study as the effective solar constant.

Eq. (4-1) was then utilized to compute the effective solar insolation at the tropopause ($k=2$) as follows:

$$F(2) = S \left[\frac{r}{r_m} \right]^{-2} \cos z \quad (4-1)$$

where S = effective solar constant at $k=2$

$\cos z$ = cosine of the zenith angle for the Julian date used

r/r_m = ratio of the actual earth-sun distance to the mean earth-sun distance for the Julian date used in this study.

The Smithsonian Meteorological Tables gives the ratio r/r_m and the solar declination δ for 16 April, 0000GMT, as these values are employed in Eq. 4-1. These values are, respectively:

$$\frac{r}{r_m} = 1.00333$$

$$\delta = 8.4833 \text{ degrees of lat.}$$

δ is used in evaluating the cosine of the solar zenith angle, given by

$$\cos z = \sin \phi \sin \delta + \cos \phi \cos \delta \cos h \quad (4-2)$$

where ϕ is the latitude and h is the hour angle of the sun for the meridional data lines. For example, Fig. 1 makes it clear that for

$$\text{line 1} \quad h = 55^\circ$$

$$\text{line 2} \quad h = 10^\circ$$

$$\text{lines 3,4} \quad h = 35^\circ$$

at the times of the synoptic charts (0000GMT and 1200GMT, as applicable). $\sin \phi$ was computed according to the standard polar stereographic projection formula applicable to the FNWC base chart given by

$$\sin \phi = \frac{r_E^2 - [(I-32)^2 + (J-32)^2]}{r_E^2 + [(I-32)^2 + (J-32)^2]} \quad (4-3)$$

where $r_E^2 = 973.752$. Thus $\sin \phi$ assumes the following functional form in terms of the FNWC grid-coordinate I (Fig. 1):

Lines 1,3,4

$$\sin \phi = \frac{973.752 - 2(32-I)^2}{973.752 + 2(32-I)^2} \quad (4-4(a))$$

Line 2

$$\sin \phi = \frac{973.752 - (32-I)^2}{973.752 + (32-I)^2} \quad (4-4(b))$$

or, conversely I is given in terms of ϕ by

$$\text{Lines 1,3,4} \quad I = 32 - 22.065 \left[\frac{\cos \phi}{1 + \sin \phi} \right] \quad (4-4(c))$$

$$\text{Line 2} \quad I = 32 - 31.205 \left[\frac{\cos \phi}{1 + \sin \phi} \right] \quad (4-4(d))$$

$I = 1, \dots, 25$ for Lines 1,2

$I = 9, \dots, 25$ for Line 3

$I = 63, \dots, 38$ for Line 4

For lines 1,2, and 3 the gridpoint soundings correspond to 0000GMT 16 April when solar noon occurs at the 180th meridian. Line 4 gridpoint soundings correspond to 1200GMT, 16 April, when solar noon was at the Greenwich meridian.

A very simple partition of solar insolation was utilized in this study after Joseph (1971). It consisted of dividing the insolation $F(2)$ into two parts at level $k=2$. One part was considered to include all wavelengths $\lambda > .9 \mu\text{m}$ where absorption by water vapor and carbon dioxide bands are the most prevalent attenuation processes in clear air. This part of the solar spectrum was termed the $F(A)$ energy and considered subject to water-vapor absorption but not to Rayleigh scattering. For those wavelengths $\lambda \leq .9 \mu\text{m}$, absorption of the solar insolation energy by water vapor was considered negligible. This part of the solar insolation was denoted $F(S)$ suggestive of the fact that it was subject only to Rayleigh scattering attenuation in clear air. The two partitions

are formulated after Joseph (1971) as follows:

$$F(A) = .349 F(2) \quad (4-5(a))$$

$$F(S) = .651 F(2) . \quad (4-5(b))$$

In this study, the introduction of two cloud decks produced cloud-reflectivity effects upon both the $F(A)$ and $F(S)$ solar energy insolutions. However, in the clear areas around any gridpoint only the absorption-attenuation applies to the $F(A)$ insolation, while only Rayleigh scattering-attenuation applies to the $F(S)$ insolation.

B. DISPOSITION OF $F(S)$ INSOLATION

In the disposition of the $F(S)$ insolation, Joseph (1971) determined that Rayleigh scattering reflectance to space by clear skies (after Coulson, 1959) could be effectively approximated by least squares in the following form

$$\alpha(R) = .085 + .25074 \left[\log \left(\frac{\pi}{P_o} \text{Sec } z \right) \right] \quad (4-6)$$

where $P_o = 1013.25$ mb. In Eq. 4-6, $\pi/P_o \doteq 1$ in view of the fact that mean sea level pressure π is close to 1000 mb.

Also

$$\text{Sec } z = (\text{Cos } z)^{-1}$$

with $\text{Cos } z$ given by Eq. 4-2.

The surface albedo $\alpha(G)$ is another reflective parameter utilized in this study. Over oceanic areas the following formula for $\alpha(G)$ after Gates et al (1971), was utilized:

$$\alpha(G) = \max \{ .06, .06 + .54 (.7 - \text{Cos } z) \} . \quad (4-7)$$

1. Clear Sky Case

In the clear sky (0,0) case the F(S) insolation was subjected to both Rayleigh scattering reflectance $\alpha(R)$ and to surface reflectance $\alpha(G)$. Considering the likelihood of a succession of multiple reflections between earth and atmosphere, the F(S) insolation actually penetrating the earth's surface after scattering is given by

$$\begin{aligned} \text{IS10}(0,0) = & F(S)[1-\alpha(R)][1+\alpha(R)\alpha(G)+\dots(\alpha(R)\alpha(G))^n \\ & +\dots]*(1-\alpha(G)) \end{aligned} \quad (4-8(a))$$

that is, by

$$\text{IS10}(0,0) = F(S)[1-\alpha(R)][1-\alpha(G)]/[1-\alpha(R)\alpha(G)] \quad (4-8(b))$$

2. Cloudy-Sky Cases

In the three cases in which clouds were present, F(S) insolation absorbed by the ground at each gridpoint was computed using the following equation (after Arakawa, 1972):

$$\begin{aligned} \text{IS10}(1,1) = & F(S)(1-R(1))(1-R(2))(1-\alpha(G)) \\ & * 1-[R(1)R(2)+R(2)\alpha(G)+R(1)\alpha(G) \\ & + 2R(1)R(2)\alpha(G)]^{-1} . \end{aligned} \quad (4-9)$$

As indicated by the notation (1,1), denoting $CL(1)=CL(2)=1.0$, Equation 4-9 is the formula used in calculating F(S) insolation absorbed by the ground in the case where overcast clouds are present at both levels of Fig. 2. Also in Eq. 4-9, constant cloud-reflectance values were chosen, namely $R(1) = .54$ for the mid-level clouds between $k=4$ and 6 , and $R(2) = .66$

for the low-level clouds between k=8 and 9. Both cloud-reflectance values are as suggested by C. D. Rodgers (1967).

For all the other cloud cases, the following changes were applied to Eq. 4-9. In the (1,0) case ($CL(1) = 1.0$, $CL(2) = 0.0$), the desired result is obtained by setting $R(2) = 0$ in (4-9), from which it follows that

$$IS10(1,0) = F(S)(1-R(1))(1-\alpha(G))/[1-R(1)\alpha(G)]. \quad (4-10)$$

In the case (0,1), one sets $R(1) = 0.0$ in (4-9) so that (4-9) simplifies to

$$IS10(0,1) = F(S)(1-R(2))(1-\alpha(G))/[1-R(2)\alpha(G)]. \quad (4-11)$$

Note that with a cloud overcast present, the Rayleigh clear-sky scattering $\alpha(R)$ does not appear in Eqs. 4-9, 4-10 or 4-11, but is included in the cloud reflectances $R(1)$ and/or $R(2)$.

3. Composite F(S) Insolation

Eqs. 4-8, 4-9, 4-10, and 4-11 were utilized in the computation of the cloud-weighted $F(S)$ insolation penetrating the earth's surface considering the areal-weights of the cloud combinations denoted by (0,0), (1,1), (1,0) and (0,1) about a gridpoint. The resultant $F(S)$ insolation penetrating the earth's surface denoted by $IS10$ is therefore expressible as

$$\begin{aligned} IS10(CL(1), CL(2)) &= IS10(0,0) W(0,0) \\ &+ IS10(1,1) W(1,1) \\ &+ IS10(1,0) W(1,0) \\ &+ IS10(0,1) W(0,1) . \end{aligned} \quad (4-12)$$

Here the weighting factors $W(0,0)$, $W(1,1)$, $W(1,0)$ and $W(0,1)$ are computed in Eqs. 2-6a, 2-6b, 2-6c, and 2-6d respectively. Note finally that the part of $F(S)$ insolation reflected to space is found by subtracting $IS10(CL(1), CL(2))$ from $F(S)$. Table VII lists the results of radiative sounding as it appears for the disposition of $F(S)$ -insolation. The individual computations of $IS10$ as they apply for the possible overcast-clear layer cases are made under the heading "IS10." The difference

$$REFS = F(S) - IS10 \quad (4-13)$$

in each case represents $F(S)$ -insolation reflected to space while

$$STRAN = \frac{REFS}{(1 - \alpha(G))} \quad (4-14)$$

has been computed as that portion of the $F(S)$ -insolation incident at the sea surface just prior to transmission by the surface. Note that no absorption in air has been included in the computations of Table VII, and that the only absorption permitted is that implicit in $IS10$. Finally at the bottom of each column, e.g., $IS10$, the composite value has been computed by means of the weighting scheme of Eq. 4-12.

CL(1),CL(2)	Weighting	IS10	REFS	STRAN
0,0	0.0	.4305	.1751	.5216
1,0	0.0	.2539	.3517	.3076
0,1	.1013	.1921	.4135	.2327
1,1	.8997	.1340	.4656	.1696
Composite F(S) values		.1452	.4603	.1760

Table VII. A sample listing of values of F(S) insolation (1y min^{-1}) computed at gridpoint (1,1) using equations detailed in Sec. IV.

C. DISPOSITION OF F(A) INSOLATION

The fractional portion of the solar insolation subject to absorption by atmospheric water-vapor and carbon dioxide are covered in the following subsections.

1. Clear-Sky Case (0,0)

The Manabe-Möller absorptivity function provided the necessary absorptivity values for the key layers in this case. The form of this absorptivity function is

$$\underline{a}(2,k) = .271[U(2,k) \text{ Sec } z]^{.303} . \quad (4-15)$$

Here \underline{a} is the absorptivity applied to the pressure-scaled water vapor mass between levels 2 and k (Fig. 2) along the zenith slant-path angle z . The resultant absorbed insolation energy in the particular layer (2-6) is then given by the Manabe-Möller relation

$$A(2,6) = 0.271F(A)[U(2,6) \text{ Sec } z]^{.303} . \quad (4-16)$$

The two layers of interest in which absorption was computed were (2,6) and (2,10). The absorbed insolation in the layer (6,10) was then computed by

$$A(6,10) = A(2,10) - A(2,6) . \quad (4-17)$$

Water-vapor mass above level 2 was assumed negligible in the F(A) disposition of the solar insolation.

By subtracting A(2,10) from F(A), the direct transmission of F(A) insolation impinging at the earth's surface was determined. The transmission of F(A) insolation is then further reduced by the transmissivity (1- $\alpha(G)$), after surface-reflectance which leads to the earth-absorbed result

$$IA10(0,0) = F(A)\{1-.271[U(2,10)\text{Sec } z]^{.303}\}(1-\alpha(G)) . \quad (4-18)$$

The transmitted energy impinging upon the earth just prior to absorption is

$$TRANA(0,0) = IA10(0,0)/[1-\alpha(G)] . \quad (4-19)$$

2. Cloudy Cases

In order to compute meaningful dispositions of F(A) insolation in cloudy-sky cases, cloud reflectivities and cloud absorptivities after C. D. Rodgers (1967) were utilized. The reflectance-values used here are different from those suggested by Rodgers for the F(S) wavelengths. The cloud reflectivities used here are RA(1) = .46 and RA(2) = .50.

In this case there are also cloud-absorptivities to be considered. These were taken as $A(1) = .20$ and $A(2) = .30$, respectively. In the following discussions the cloud conditions are considered totally overcast in each of layers indicated when the notations $((1,1), (0,1)$ and $(1,0))$ are utilized.

Schematic representation of the computations performed in the various cases $((1,1), (0,1), (1,0))$ are displayed in Fig. 3. This figure indicates the theoretical parameters required in computing the disposition of incoming $F(A)$ -insolation from level $k=2$ to the earth's surface ($k=10$). The equations which relate to the parameters in Fig. 3 and the other cloud configurations are listed in Appendix B of Spaeth's study (1975).

The insolutions, A_{24} , A_{46} , A_{68} , A_{89} and A_{910} , etc., represent the contributions to the insolation absorbed in the layers $(2,6)$ and $(6,10)$ involved. Symbols F_2 , F_4 , F_6 , F_8 and F_9 , etc., depict the streams of insolation passing through the indicated level. A vertical arrow implies the direction of insolation passage, i.e., \downarrow denotes downward insolation, \uparrow upward-reflected insolation, and $\downarrow\downarrow$ downward-reflected insolation. The absorption quantity $A(6,8)\downarrow\downarrow$, for example, indicates absorbed energy remaining in $(6,8)$ from a downward reflected beam.

Since multiple reflections occur between the earth's surface and a cloud base, or between cloud-layers in this

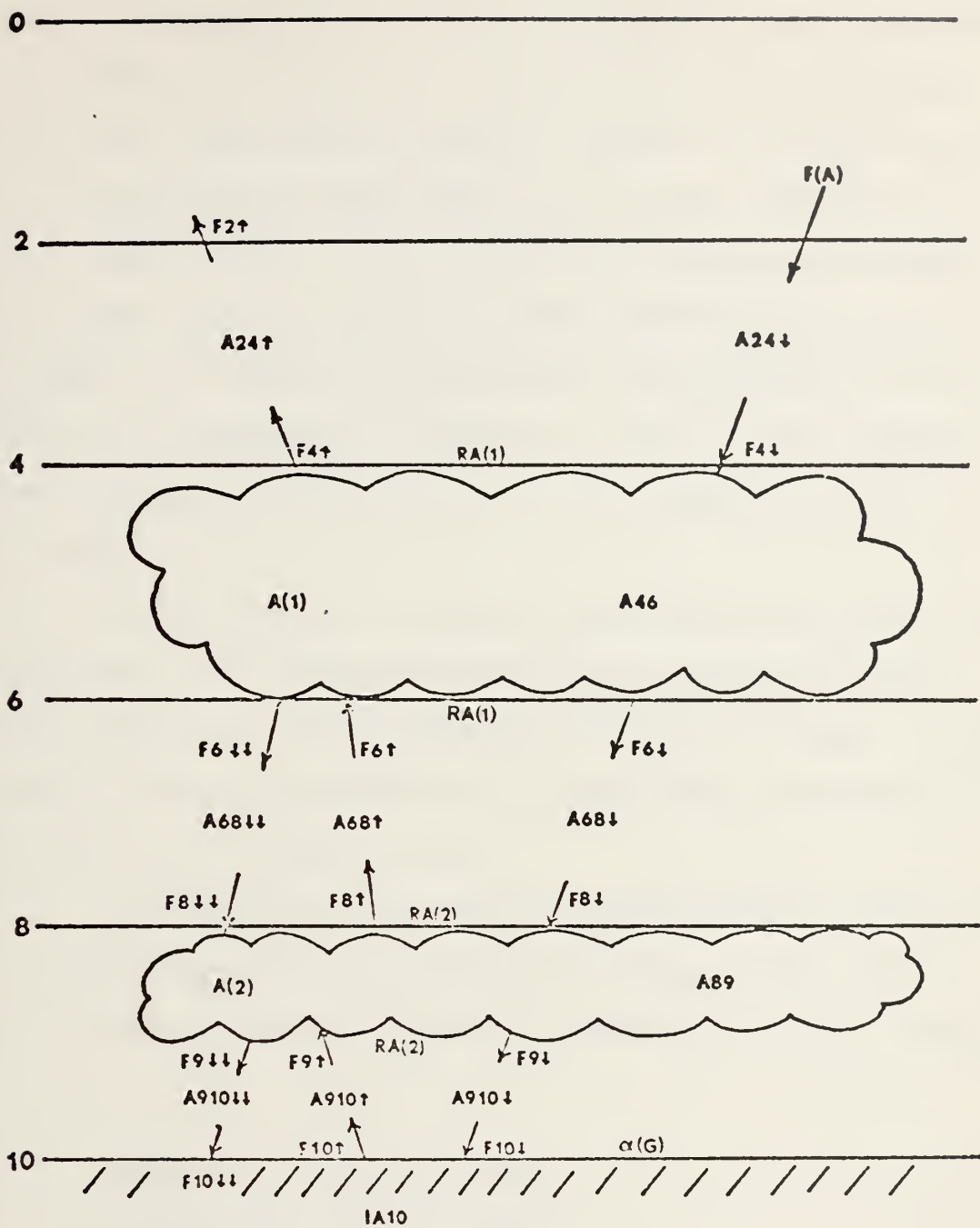


Figure 3. Schematic representation of $F(A)$ insolation disposition in the case of two overcast layers(case(1,1)).

model, the insolation amount reaching the lowermost reflecting surface is affected by the downward reflected beams. Additional insolation amounts remaining after more than two reflections are negligible, and are not included in the model computations. Thus, note that insolation reflected upward from a lower interface, either cloud-top or ground, to the base of a higher cloud deck was not subjected to absorption by or transmission through the cloud. This simplification resulted in slightly reduced $F(A)$ insolation-reflectance to space.

A final point to note is that there are three contributions to the absorption of solar insolation within a layer between any two reflecting surfaces. In Fig. 3 these contributions are identified by arrows which indicate the portion of path being crossed.

For each of the possible overcast-cloud combinations, the transmitted $F(A)$ insolation arriving at the earth's surface may be defined using the following notation (TRANA) as

$$\text{TRANA}(1,1) = F_{10\downarrow} + F_{10\downarrow\downarrow} \quad (4-20)$$

$$\text{TRANA}(1,0) = F_{10\downarrow} + F_{10\downarrow\downarrow} \quad (4-21)$$

$$\text{TRANA}(0,1) = F_{10\downarrow} + F_{10\downarrow\downarrow} \quad (4-22)$$

where the right side parameters of (4-20), (4-21), and (4-22) are derived in Appendix B of Spaeth (1975).

The $F(A)$ insolation absorbed by the earth in each cloud-case considered is derived from

$$IA10(1,1) = F10\downarrow (1-\alpha(G)) + F10\uparrow\downarrow \quad (4-23)$$

$$IA10(1,0) = F10\downarrow (1-\alpha(G)) + F10\uparrow\downarrow \quad (4-24)$$

$$IA10(0,1) = F10\downarrow (1-\alpha(G)) + F10\uparrow\downarrow \quad (4-25)$$

In the last three equations, the quantity $F10\uparrow\downarrow$ is small enough in each case, that no further reflections from the earth were considered.

3. Composite $F(A)$ Layer-Absorptions and Surface-Absorption Insolation

As has been previously discussed, the standard grid-area weighting scheme of this study was applied to obtain composite values of the absorbed $F(A)$ -insolation in key layers and also within the earth's surface. The weighting factors applied to the corresponding overcast-combination absorption quantities provided the following composite results:

$$\begin{aligned} A26(CL(1), CL(2)) &= A26(0,0)W(0,0)+A26(1,0)W(1,0) \\ &+ A26(0,1)W(0,1) \\ &+ A26(1,1)W(1,1) \end{aligned} \quad (4-26)$$

$$\begin{aligned} A610(CL(1), CL(2)) &= A610(0,0)W(0,0)+A610(1,0)W(1,0) \\ &+ A610(0,1)W(0,1) \\ &+ A610(1,1)W(1,1) \end{aligned} \quad (4-27)$$

$$\begin{aligned} IA10(CL(1), CL(2)) &= IA10(0,0)W(0,0)+IA10(1,0)W(1,0) \\ &+ IA10(0,1)W(0,1) \\ &+ IA10(1,1)W(1,1) \end{aligned} \quad (4-28)$$

The weighting factors $W(0,0), \dots, W(1,1)$ were first listed in Eqs. 2-6(a,b,c,d). Also $A26(0,0)$, $A610(0,0)$, $IA10(0,0)$ are given in each clear-sky case (0,0) about each gridpoint by Eqs. 4-16, 4-17 and 4-18, respectively.

The results for the absorption in layers (2,6), (6, 10) and at the surface are shown in the following table for the four cloud cases [(0,0), (1,0), (0,1), (1,1)] and for the composite cases based on the weighting factors (also listed).

CL(1),CL(2)	Weighting	A26	A610	AI10	REFA	TRANA
0,0	0.0	.0809	.0804	.1348	.1751	.7069
1,0	0.0	.1192	.0436	.0482	.3517	.3774
0,1	.1013	.0845	.1499	.0238	.4140	.2697
1,1	.8987	.1192	.0717	.0104	.4656	.1880
Composite values		.1157	.0797	.0118	.4603	.1962

Table VIII. A sample listing of gridpoint values (1y (min)^{-1}) of $F(A)$ insolation computed at gridpoint (1,1) using Eqs. 4-26, 4-27 and 4-28.

In the computational scheme indicated by the entries of Table VIII, the reflected $F(A)$ insolation to space has been depicted by the symbol REFA, and its values follow from

$$REFA = F(A) - A26 - A610 - IA10 \quad (4-29)$$

whereas the TRANA dispositions are given by Eqs. 4-19, ..., 4-22, respectively, or by its weighted-mean value in the case of TRANA-composite.

4. Absorptivity (ABA) by Layers

Here the (fractional) absorptivity as well as the actual insolation values absorbed in the layers are considered. In the computation of absorptivity, which is fractional absorption, the total undepleted insolation at the top ($k=0$) is used as a base. The following equation was utilized in this calculation:

$$FADJ = 2.00(r/r_m)^{-2} \cos z . \quad (4-30)$$

The absorptivity of the troposphere ABA was computed from the ratio of the insolation absorbed in the troposphere to the insolation incident at the top of the atmosphere rather than at $k=2$:

$$ABA = \frac{A(2,6) + A(6,10)}{FADJ} . \quad (4-31)$$

D. ALBEDO (ALB) OF THE EARTH-TROPOSPHERE SYSTEM

In considering the planetary albedo, the reflected insulations of the earth-troposphere system in both the $F(A)$ and $F(S)$ insolational regions must be recalled by the program. Thus REF is computed at each gridpoint as the sum of the reflected insolation energy in $F(A)$, denoted REFA in Eq. 4-29 and the reflected part of $F(S)$ (denoted REFS in Eq. 4-13):

$$REF = REFS + REFA . \quad (4-32)$$

Finally the planetary albedo is related to FADJ through

$$ALB = \frac{REF}{FADJ} . \quad (4-33)$$

E. COMPOSITE ABSORPTIVITY (ABG) BY THE EARTH-SURFACE;
COMPOSITE ATMOSPHERIC TRANSMISSIVITY (ATRAN)

1. Absorptivity (ABG) of Earth

By summing the weighted values of F(S) and F(A) portions of the incoming insolation entering the earth, the total insolation absorbed at the earth's surface was computed. This quantity when divided by the extraterrestrial insolation gave the fractional absorptivity (ABG) of the earth's surface. The equation for ABG was

$$ABG = \frac{IA10 + IS10}{FADJ} \quad (4-34)$$

where IA10, IS10, and FADJ were defined previously by Eqs. 4-28, 4-12, and 4-30, respectively.

2. Transmissivity (ATRAN) of the Troposphere

Also computed was the total insolational energy TRAN, incident at the earth's surface just before absorption by the surface. This calculation is given by

$$TRAN = TRANA + STRAN . \quad (4-35)$$

Here $STRAN = [IS10/(1-\alpha(G))]$ was previously defined in Eq. 4-14, and $\alpha(G)$ was given in Eq. 4-7. TRANA has also been defined as the weighted value of $TRANA(0,0)$, $TRANA(1,1)$, $TRANA(1,0)$ and $TRANA(0,1)$ given by Eqs. 4-19, 4-20, 4-21, and 4-22. Note also in justification of STRAN that the four cases for IS10 of (4-8), (4-9), (4-10), and (4-11) each have the common factor $(1-\alpha(G))$ in the numerator and therefore

each transmitted $F(S)$ insolation component available at the earth just before absorption needs only be divided by $(1-\alpha(G))$. TRAN may thus be viewed as the total insolational energy incident at a pyrheliometer located at earth. The (fractional) transmissivity of the troposphere (ATRAN) is then computed from

$$\text{ATRAN} \equiv \text{TRAN} / \text{FADJ} . \quad (4-36)$$

Note finally that the major dispositions of the total insolation at the indicated map times have now been identified by the fractional values, ALB, ABA or ABG, and ATRAN, representing the reflectivity (albedo), absorptivity of air or earth, or atmospheric transmissivity as the case may be.

3. Computational Check

The computational scheme utilized in this model was checked continuously by summing the fractional values ALB, ABA, and ABG at each gridpoint. The value in each case must total .96, since as previously noted the attenuation of solar insolation was taken as four percent as it passed through the stratosphere.

F. STATISTICAL ANALYSIS

In order to substantiate some of the computations performed in this section, several of the most important items computed were statistically analyzed using linear regression computer programs from the BMD set of statistical programs (Dixon, 1973).

1. Clear Sky Cases

Using ALB (0,0,z), which is the clear sky case of albedo, as the predictand, and $\log_{10} \text{Sec } z$ as the predictor, the following best-fit equation resulted

$$\begin{aligned} \text{ALB}(0,0,z) &= .07734 + .40072 \log_{10} \text{Sec } z \\ R_M &= .9624 \end{aligned} \quad (4-37)$$

where R_M represents the multiple correlation coefficient.

This result was as expected over the ocean where $\alpha(G)$ and $\alpha(R)$ involved logarithmic dependence on $\text{Sec } z$. The sample average values of ALB and $\log_{10} \text{Sec } z$ were

$$\overline{\text{ALB}(0,0)} = .1358 \quad \overline{\log_{10} \text{Sec } z} = .1459 .$$

Other clear-sky regression tests made use of the water-vapor mass path length (M) defined by

$$M = (U \text{ Sec } z)^{1/2} \log_{10} (U \text{ Sec } z) . \quad (4-38)$$

This parameterization of water vapor mass is similar to that developed by Hanson (1971), who used a similar M as a predictor in his empirical formulations of ABA for both clear and partly cloudy sky cases. In this study the two regressions attempted using M as a predictor were with ABA(0,0,M) and ATRAN(0,0,M) as predictands. The best-fit equations resulting were

$$\text{ABA}(0,0,M) = .09572 + .03136M \quad (4-39)$$

$$R_M = .9875$$

$$\text{ATRAN}(0,0,M) = .79520 - .03182M \quad (4-40)$$

$$R_M = .9488 .$$

The absorptivity in the form given by (4-39) agrees closely in form with that obtained by Spaeth based on 16 January 1974 data and with that of Quinn based on pyrliometric data (1971).

The means of $ABA(0,0,M)$ and $ATRAN(0,0,M)$ for the original 93 gridpoint sample were

$$\overline{ABA(0,0,M)} = .13459$$

$$ATRAN(0,0,M) = .75576$$

$$\bar{M} = 1.23945 \text{ (gm cm}^{-2}\text{)}^{1/2} .$$

2. Statistical Relationships Between ALB, ABA and ATRAN in the Cloudy and Clear Sky Cases

In addition to computing the clear-sky value of ALB, it was also possible to compute the composite cloud value of ALB. A regression was formed showing the relationship between the ratio $ALB(CL(1),CL(2))/ALB(0,0)$ as the predictand and the total opaque cloud cover (CL) as the predictor. CL in this model is specified by Eq. 3-12. CL, it was felt, gave a good approximation of the effective cloud-cover by the two layers of cloud amounts CL_1 and CL_2 by Eq. 2-4 used in this model. As explained earlier in this study, a one-third reduction of both $CL(1)$ and $CL(2)$ after initial determination by Eq. 2-4 was also tried in all computations involving cloud amounts. This test represented an attempt at tuning the cloud model for radiative calculations, and gave results in closer agreement with the latest literature on satellite reflectances. Thus all subsequent regressions of ALB, etc.

upon CL, after Eq. 2-4, will also include those best-fit equations formulated using a CL' based upon Eqs. 2-5 and 3-12. A small letter subscript 'a' in the equation number will indicate those computations using 2/3-CL amounts while a small letter subscript 'b' will indicate those utilizing full-CL cloud model amounts.

The first regression equations tested were those for ALB(CL) and ABA(CL) for the respective cases of 2/3-CL and full-CL cases. The results are given in (4-41(a)), (4-41(b)). The symbol R_M once again signifies the multiple correlation of the statistical regressions.

$$\begin{aligned} \text{ALB}_a(\text{CL}(1)\text{CL}(2)) &= \text{ALB}(0,0)[1 + 4.7154\text{CL} \\ &\quad - 2.3648\text{CL}^2] \end{aligned} \quad (4-41(a))$$

$$R_M = .9640$$

$$\begin{aligned} \text{ALB}_b(\text{CL}(1)\text{CL}(2)) &= \text{ALB}(0,0)[1 + 4.7273\text{CL} \\ &\quad - 1.6974\text{CL}^2] \end{aligned} \quad (4-41(b))$$

$$R_M = .9670$$

The sample means of the values in Eqs. 4-41a and 4-41b are

Eq. 4-41a

$$\overline{\text{ALB}(\text{CL}(1),\text{CL}(2))} = .3624$$

$$\overline{\text{ALB}(0,0)} = .1358$$

$$\overline{\text{CL}} = .5876$$

Eq. 4-41b

$$\overline{\text{ALB}(\text{CL}(1),\text{CL}(2))} = .4473$$

$$\overline{\text{ALB}(0,0)} = .1358$$

$$\overline{\text{CL}} = .7746$$

The high value of the correlation coefficient in Eq. 4-41 shows strong dependence of ALB upon CL in either cloud

parameterization case. Also note that ALB(CL(1),CL(2)) values computed here are clearly higher than reported by Raschke et al, (1973), where ALB = .25 for essentially the same set of gridpoints during the NIMBUS III period 1-15 May 1969. The 2/3-CL cloud parameterization gives albedo results which are closer to Raschke's results, suggesting that the full-CL amounts of Smagorinsky (Eq. 2-4) are too high for radiational computations.

A second regression was developed between ABA(CL) /ABA(0,0) versus CL. The following best-fit equations results:

$$\begin{aligned} \text{ABA}_a(\text{CL}(1),\text{CL}(2)) &= \text{ABA}(0,0)[1 + .5873\text{CL} \\ &\quad - .1018\text{CL}^2] \end{aligned} \quad (4-42(a))$$

$$R_M = .8956$$

$$\begin{aligned} \text{ABA}_b(\text{CL}(1),\text{CL}(2)) &= \text{ABA}(0,0)[1 + .6526\text{CL} \\ &\quad - .1481\text{CL}^2] \end{aligned} \quad (4-42(b))$$

$$R_M = .9012$$

Mean statistics for this regression case are

Eq. 4-42a	Eq. 4-42b
$\overline{\text{ABA}_a(\text{CL}(1),\text{CL}(2))} = .1758$	$\overline{\text{ABA}_b(\text{CL}(1),\text{CL}(2))} = .1894$
$\overline{\text{ABA}(0,0)} = .1346$	$\overline{\text{ABA}(0,0)} = .1346$
$\overline{\text{CL}_a} = .5876$	$\overline{\text{CL}_b} = .7746$

From the means of (4-42), it is seen that the model specifies an increase in atmospheric (solar) absorptivity with increasing cloud cover. This result is in agreement with studies

of Warner (1974) and Spaeth (1975) and with the earlier study of London (1957).

An analogous statistical regression was then developed for the cloudy-sky transmissivity relative to the clear-sky transmissivity. The resulting regressions were

$$\begin{aligned} \text{ATRAN}_a(\text{CL}(1), \text{CL}(2)) &= \text{ATRAN}(0,0)[1 - .6581\text{CL}] \\ R_M &= .9992 \quad (4-43(a)) \end{aligned}$$

$$\begin{aligned} \text{ATRAN}_b(\text{CL}(1), \text{CL}(2)) &= \text{ATRAN}(0,0)[1 - .6833\text{CL}] \\ R_M &= .9986 \quad (4-43(b)) \end{aligned}$$

with sample mean values as follows:

Eq. 4-43a	Eq. 4-43b
$\frac{\text{ATRAN}_a(\text{CL}(1), \text{CL}(2))}{\text{ATRAN}(0,0)} = .4653$	$\frac{\text{ATRAN}_b(\text{CL}(1), \text{CL}(2))}{\text{ATRAN}(0,0)} = .3589$
$\quad \quad \quad = .7558$	$\quad \quad \quad = .7558$

The parameter $\text{ATRAN}(\text{CL}')/\text{ATRAN}(0,0)$ given by (4-43a) is in very good agreement with the statistical result of Savino-Angstrom from earth-based pyrliometry at Canton Island, which was

$$Q = Q_0 (1 - .655\text{CL})$$

(Budyko, 1958). The coefficient of CL in this result is known to be a slowly decreasing function of latitude.

Similarly, the parameters $\text{ALB}(\text{CL}')/\text{ALB}(0,0)$ and $\text{ABA}(\text{CL}')/\text{ABA}(0,0)$ behave consistently with respect to increasing CL, with more realistic mean values for $\overline{\text{ALB}(\text{CL}')}$ and

ABA(CL') than for the corresponding full-CL parameterization. Hence, in the mean, the statistical analyses performed seem to show agreement with observational results of other investigators. Comparative computations of the atmospheric transmissivity, particularly in the 2/3-CL case appear to give better agreement with ground-based pyrheliometry.

A major test still to be made is the comparison of the latitudinal-distribution of $ALB_a(CL)$ and $ALB_b(CL)$ with that of the satellite albedo of Raschke et al (1973).

G. ALBEDO COMPARISONS WITH PUBLISHED RESULTS

The tropospheric albedo computations of the solar-insolation model of this section have been presented for both the full-cloud and two-thirds CL cases, respectively. These albedos have been interpolated to whole multiples of 5° latitude between $20^\circ S$ and $65^\circ N$. These computations were made for each of the four oceanic meridians and the resulting albedos averaged across the meridians are presented as a function of latitude in Table IX for both the full-CL and two-thirds CL cases, where comparison is also made with satellite albedos of Raschke et al (1973), for the NIMBUS III period 1-15 May 1969. For sake of consistency the Raschke albedo data have been extracted from atlas presentations to the 5 degree latitude grids, on the same four meridians, before applying the same averaging process.

The model results under the headings "FULL-CL" and "2/3-CL" correspond to the composite cloud amounts previously listed in Table V according to the Eq. 3-12.

The most unusual results to be observed in Table IX are the small albedo-values ($\approx .2$) between 20S to 20N, after Raschke, as contrasted with the corresponding values (in the range .3 to .47) by the 2/3-CL model, and more markedly with those by the full-CL model (values in the range .43 to .59). The cosine-weighted mean albedos (see Eq. 7-2) are as follows:

$$\text{FULL-CL, } \overline{\text{ALB}} = .46$$

$$\text{2/3-CL, } \overline{\text{ALB}} = .37$$

$$\text{RASCHKE-ALB} = .25$$

At every latitude ($\phi \leq 60$) under comparison the 2/3-CL albedo computation is closer to Raschke's observations than is the full-CL value so that there is no question in accepting the 2/3-CL over the full-CL case. At latitude $\phi = 65$, there is evidence of added surface-ice reflections contributing to the Raschke value of planetary albedo. For example at latitude 65N Raschke's results indicate $\text{ALB} = .5$, whereas the 2/3-CL model computations with a rather high cloud cover ($\text{CL}' = .79$) is .47. Part of this discrepancy with the solar radiation model at high latitudes lies in the non-inclusion of a surface-ice reflectance parameter.

To summarize, apart from the region covered by sea-ice, there is a marked preference for the 2/3-CL over the full-CL model in giving albedos closer to those observed by satellite for the same general period (1-15 May 1969) as reported by Raschke et al (1973) and Von der Haar and Hanson

Lat.	ALBEDO			MODEL	
			(Raschke)	Cloud-Amount	
	(Full-CL)	(2/3-CL)		(Full-CL)	(2/3-CL)
20S	.568	.473	.17	.985	.842
15	.559	.462	.17	.983	.828
10	.512	.418	.18	.944	.752
5	.446	.363	.20	.842	.647
0	.475	.374	.21	.878	.659
5	.443	.347	.22	.829	.591
10	.438	.337	.20	.823	.639
15	.434	.333	.19	.799	.548
20	.430	.331	.18	.788	.536
25	.381	.314	.20	.642	.473
30	.351	.298	.24	.582	.446
35	.361	.316	.29	.634	.520
40	.372	.311	.28	.630	.468
45	.414	.336	.30	.630	.467
50	.499	.415	.33	.877	.674
55	.443	.383	.40	.719	.555
60	.562	.493	.42	.962	.816
65N	.609	.474	.50	.995	.796
Wt Avg	.458	.373	.24	.796	.596

Table IX. Comparison of planetary albedo as found by this study for both full- and two-thirds cloud models for 16 April 1974, and by Raschke et al (1973) based upon NIMBUS III measurements. Also included are the globally-weighted mean values at the bottom of each tabular column and the composite cloud amounts for both cloud cases.

(1969) and others. The primary difficulty even with the 2/3-model occurs in tropical and subtropical latitudes where Von der Haar and Hanson (1969) have discussed the reality of even smaller than suspected cloud-covers and smaller values of the resultant global-albedo. At these latitudes (tropical and subtropical) it seems doubtful that a large-scale CL-parameterization of the Smagorinsky type will be applicable. Rather some method of specifying the distribution at gridpoints of isolated cumulus towers may be appropriate. Finally, it is open to question whether vertically-structured convective cloud elements will have the high reflective capability attributed to clouds which are depicted as existing in horizontal layers with a constant reflectivity $.5 \leq R \leq .65$ as specified in the radiation model. It may well be that the vertical shafts between convective elements may be a more efficient focus for solar energy to the earth than is perceived by ascribing to the cloud amount a constant cloud albedo value. A more realistic approach may be to reduce the two-cloud layering in the tropics to clouds existing in a single layer.

At any rate with the two layered cloud-model considered in this study, the only feasible choice is the 2/3-CL parameterization. This selection is carried over into the computations of Section VI. A further test of the cloud-parameterization effect on the computation of net radiation of the earth-atmosphere system, by comparison with that observed by satellite, is made in Section VII.D.

V. SENSIBLE AND LATENT HEAT TRANSPORT AT THE SEA-AIR INTERFACE

A. GENERAL PURPOSE

The model used here to describe the turbulent transports of sensible and latent heat across the sea-air interface was basically that already in use in the operational FNWC primitive equation model. This model has been discussed in detail by Kesel and Winninghoff (1972) and by Kaitala (1974). The primary purpose of the adaptation of the turbulent flux model in this study was to test the magnitudes and directions of these transfer rates in comparison with those of the radiational transfer model discussed here in Sections III and IV. The final purpose of the inclusion of the turbulent flux model was to conduct a diagnostic computation of the heat balance within the oceanic and atmospheric layers for 16 April 1974 under the combined operation of the radiational and turbulent flux models.

B. WINDSPEED COMPUTATION IN THE TURBULENT FLUX MODEL

At all of the 93 gridpoints tested, the geostrophic wind-speed V_g was computed by use of the standard formula

$$V_g = \frac{g}{f} \frac{\Delta Z}{2(d/m)} \quad (5-1)$$

with

$$f = \left(\frac{4\pi}{86,400} \right) \sin \phi \quad (5-2)$$

$$m = \frac{1.86603}{1 + \sin \phi}$$

and

$$\Delta Z = \sqrt{(Z_4 - Z_2)^2 + (Z_3 - Z_1)^2} \quad (5-3)$$

In Eq. 5-1, $d = 381.0\text{km}$ is the nominal FNWC grid-spacing (true at 60°N) and $(\frac{2d}{m})$ is the true earth spacing used in the centered-difference computations of the contour gradient (cf., Fig. 3).

In Eqs. 5-1 and 5-3 ΔZ is the contour-difference, centered in most cases on the gridpoint under consideration. However, at the map edge gridpoints of the meridians, it was only possible to compute a forward-differenced version of V_g (cf., Fig. 4). Thus at edge-point "0", Eq. 5-4 below was used. The spacing $\frac{d}{m}$ in Eq. 5-4 is then taken as one-half that in (5-1), so that

$$V_g = \frac{g}{f} \frac{\Delta Z}{(d/m)} \quad (5-4)$$

with

$$\Delta Z = \sqrt{(Z_4 - Z_0)^2 + (Z_3 - Z_0)^2} \quad (5-5)$$

All geostrophic windspeeds were then converted to surface windspeeds using the following empiricism due to Langlois and Kwok, (1969)

$$V_s = .8 V_g + 2.2 \quad (5-6)$$

where V_s = surface windspeed (mps) and V_g is the 1000mb geostrophic windspeed. The factor 2.2 in (5-6) is an empiricism introduced to include the effects of gustiness upon the

measured (steady-state) windspeed.

In the interval of ± 10 degrees of latitude, the value of the Coriolis parameter was arbitrarily set at $f = \pm .25 \times 10^{-4} \text{sec}^{-1}$, following Kaitala (1974), while for $|\phi| > 10$ degrees the actual value of f for the particular latitude was used.

C. SENSIBLE HEAT TRANSPORT

The details of the adaptation of the FNWC model for sensible heat transport H_T utilized in this study follow the description of Spaeth (1975). The formulation of H_T is given below in terms of bulk parameters of the surface and of the planetary boundary layer (10,8) of Figs. 2 and 5:

$$H_T = \rho_{10} C_p C_D V_s (T_g - T_x) \quad (5-7)$$

$$\rho_{10} = \rho_{10} (R_d T_{10})^{-1}$$

where

$$C_p = .239 \text{ cal gm}^{-1} (\text{deg.K})^{-1}$$

and

$$C_D = 1.4 \times 10^{-3} \text{ (after Weiler and Burling, 1967)}$$

The equation utilized in this study to compute T_x may be shown to be (Spaeth, 1975)

$$T_x = \frac{C_D V_s T_g + \frac{2 \tilde{K} \theta_g}{\Delta Z} - 2 \tilde{K} \gamma_c}{\frac{2 \tilde{K}}{\Delta Z} + C_D V_s} \quad (5-8)$$

where

$$\theta_9 = T_9 \left(\frac{1000}{900} \right)^{.286} \quad (5-9)$$

$$\tilde{K} = \frac{K^*}{1 + a^* \left(\frac{\theta_9 - \theta_g}{Z_9 - Z_{10}} \right)} \quad (5-10)$$

$$\Delta Z = Z_9 - Z_{10} = \frac{R_d}{g} T \left(\ln \frac{10}{9} \right) \quad (5-11)$$

In Eq. 5-10, the turbulent parameters K^* and a^* have been determined empirically by FNWC

$$K^* \doteq 10^5 \text{ cm}^2 \text{ sec}^{-1}$$

$$a^* \doteq 5 \times 10^4 \text{ cm}(\text{deg.k})^{-1} .$$

$T_g - T_x$ in Eq. 5-7 is the temperature change for the thin layer between the surface and the top of the constant flux layer (cf., Fig. 5(a)). The formula for T_x deduced here required a constant value of sensible heat H_Γ then decreasing linearly with pressure to $H_\Gamma = 0$ at $k=8$, and remaining zero above $k=8$. This linear decrease of H_Γ with pressure is compatible with the condition of constant convergence of the sensible heat flux per gram in the turbulent boundary layer (x,8). Thus, the constant value of the convergence of sensible heat as given by Eq. 5-7 within the layer (8,10) may then be considered to be applicable at level $k=9$ as depicted in Fig. 5(a), after Spaeth (1975).

After computing T_x by Eq. 5-8, H_Γ was then computed at each gridpoint using the bulk transfer equation 5-7. The

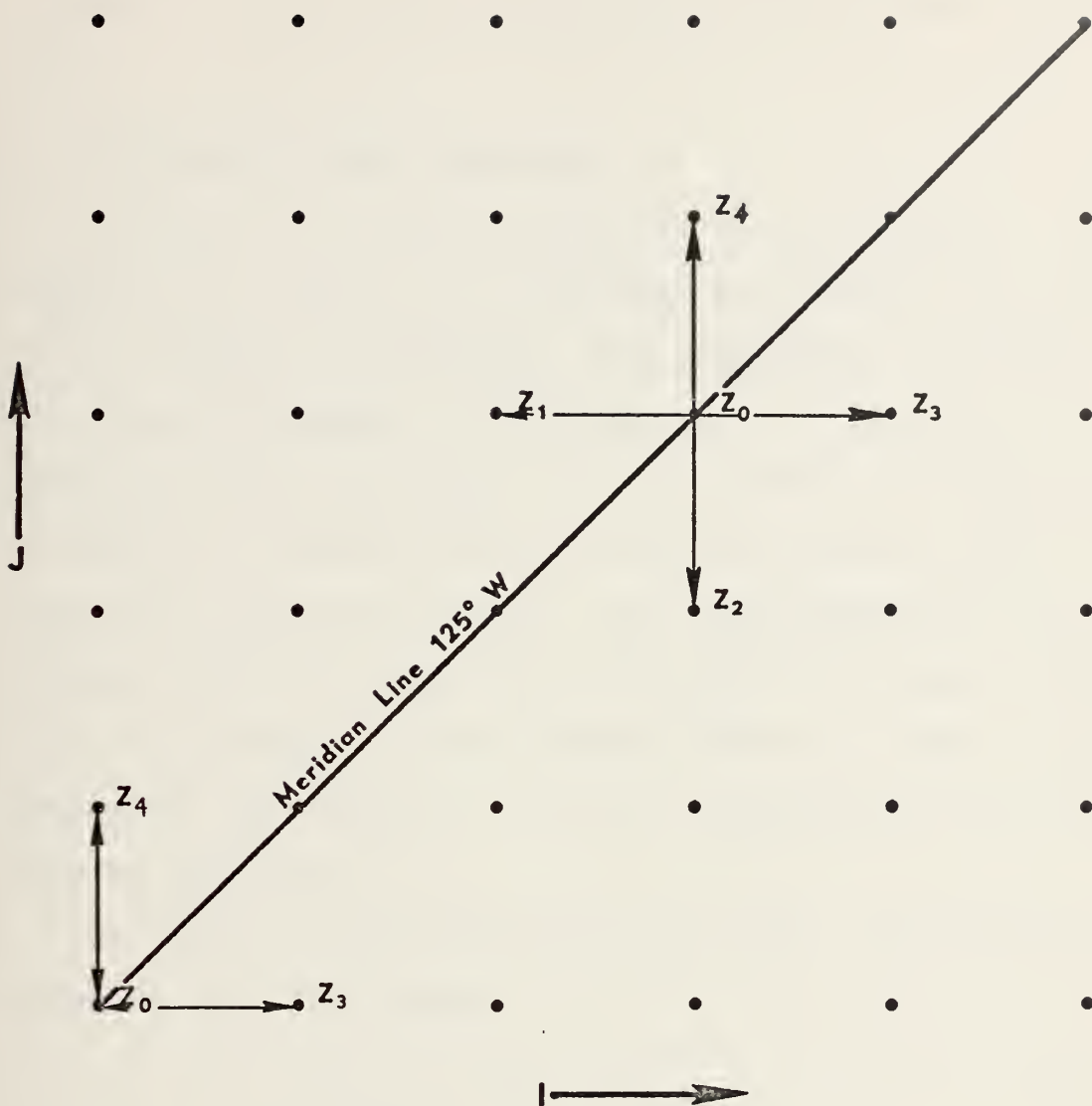


Figure 4. Section of FNWC polar stereographic meridian illustrating the method of obtaining contour gradients in the vicinity of a gridpoint. The values of contour-heights correspond to the 1000 mb D-values in the neighborhood of the gridpoint.

gridpoint values of H_T are used later in calculations of atmospheric and oceanic heat balances in Sections VI and VIII.

D. EVAPORATIVE HEAT TRANSPORT

Similar to the case of sensible heat convergence, the latent heat transport by turbulence was assumed to be subject to constant evaporative flux convergence throughout the layer 800-1000mb. The total amount of latent heat removed by evaporation from the ocean surface was essentially as modeled by Kaitala (1974) using bulk-transfer theory. It should be recognized however, that the condensation and consequent realized latent heat may occur at arbitrary levels, i.e., in general at levels higher than $k=8$. Thus, in following the FNWC model, we have not introduced E as a heating rate at level $k=9$.

The basis of the turbulent latent heat model adopted is shown in Fig. 5(c), where

$$E_{(900)} = 1/2 E (\text{Bulk}) \quad (5-12)$$

and where the surface layer bulk transfer of latent heat is given by

$$E \equiv E(\text{Bulk}) = L\rho_{10} C_D V_s (q_s - q_x) . \quad (5-13)$$

Evaporation at level $k=9$ may also be computed using

$$E_{(900)} = L\rho_{10} \tilde{K} \frac{(q_x - q_9)}{(z_9 - z_{10})} \quad (5-14)$$

where \tilde{K} is given in Eq. 5-10.

In (5-13) and (5-14) L is the latent heat of vaporization.

$$L = 596.73 - 601T_{10}$$

in $\text{cal}(\text{gm})^{-1}$. In (5-13) and (5-14) q_9 and q_x are the mixing ratios at the levels $k=9$ and at x , respectively. The factor $1/2$ which appears in the right side of (5-12) re-emphasizes the concept of constant latent-heat convergence in the level $(x,8)$, (cf., Fig. 5(c)).

The solution for q_x is obtained by combining Eqs. 5-12, 5-13 and 5-14 in the form

$$q_x = \frac{C_D V_s q_{10} + 2 \frac{\tilde{K}}{\Delta Z} q_9}{C_D V_s + 2 \frac{\tilde{K}}{\Delta Z}} \quad (5-15)$$

where $\Delta Z = Z_9 - Z_{10}$.

Applications of Eqs. 5-13 and 5-15 make possible the computation of E at each gridpoint. As in the case for T_x , the factor of $2\tilde{K}$ of (5-15) was taken to conform to the value \tilde{K} as used by Kaitala (1974) so that the turbulent transport results obtained here will be compatible with those computed operationally by the FNWC primitive equation model. As already noted, this was accomplished in this study by using a value of $2K^* = 2 \times 10^5 \text{ cm}^2 \text{ sec}^{-1}$ as equivalent to the K^* -value of Kaitala (1974). Thus computations of E by Eqs. 5-13 and 5-15 were equivalent to that using Kaitala's scheme (1974), the only change being that the vertical distribution of E implicit in Fig. 5(b) is slightly different from that

of the constancy of E everywhere in the planetary boundary layer, as postulated by Kaitala (1974).

E. TURBULENT HEAT TRANSPORTS OVER AN ICE-COVERED OCEAN

Though this study did not have any data taken from an ice-covered ocean, it should be noted that Spaeth (1975) devised an acceptable method of handling this realistic consideration, which would be applicable if our computations extended beyond the poleward limit of this study which was established at $\phi = 65\text{N}$.

F. LARGE-SCALE TURBULENT HEAT FLUX ACROSS THE SEA-AIR INTERFACE

As shown in Section VI, the combination of $E + H_T$ turns out to be a heat loss mechanism at the ocean surface, as computed at each gridpoint. The values of H_T which represent the sensible heating rates for the atmospheric layer (8,10) were computed for each gridpoint along the four meridians. The values of H_T in general turned out to be small and negative in low latitudes, reflecting the computed negative values of $T_g - T_x$, as also reported by Spaeth (1975). In the mid-latitudes, where $T_g - T_x > 0$, H_T was positive and therefore contributes positively to the net atmospheric temperature changes in the layer (8,10). The latent heat term (E) was dominantly large and positive relative to H_T throughout this study. Thus, regardless of possible inconsistencies in the sign of H_T , combined values of $E + H_T$ seemed to give reasonable heat-loss rates at the ocean surface at all latitudes, as also found by Spaeth (1975).

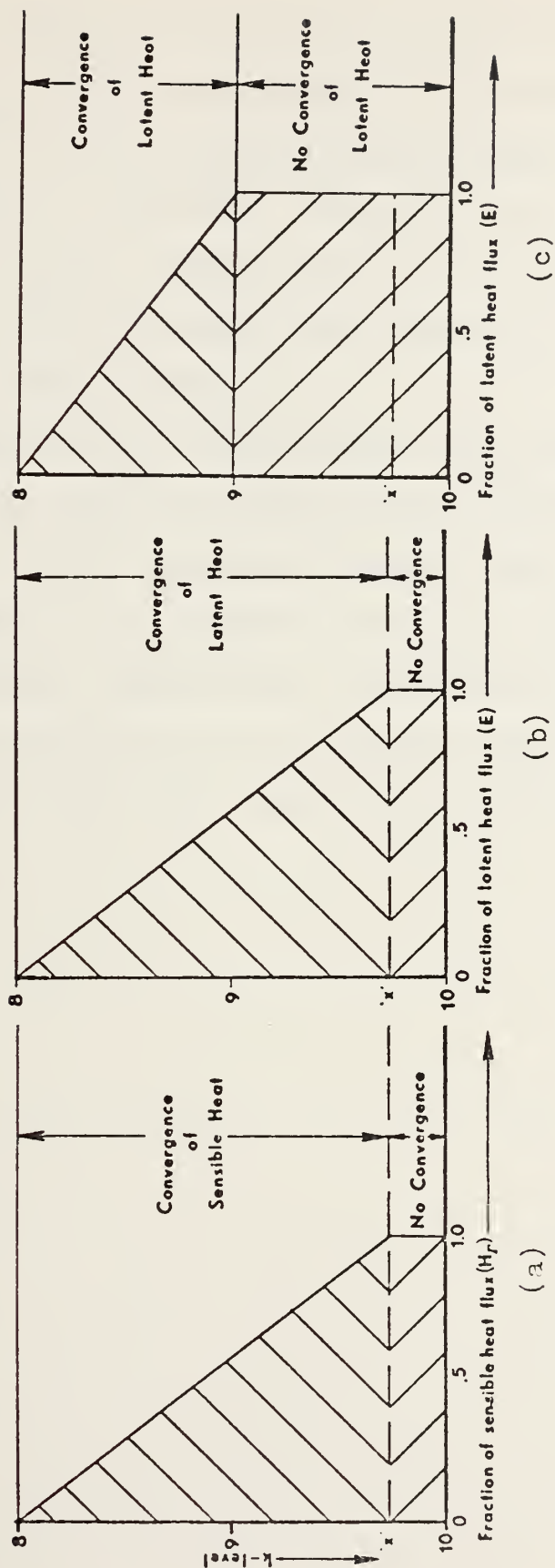


Figure 5. Schematic representation of the distribution of convergence of sensible heat used in this study (a), latent-heat used in this study (b), and latent-heat flux after Kaitala (1974) (c). Note 'x' is the level of the top of the constant flux layer.

In the large-scale sense $E + H_T$ is included as a positive contribution to the heat budget of the tropospheric column, even though it is not known precisely where the latent heat source E will be realized. The use of the equations of conservation of mass, momentum and of water-vapor mass, would resolve the latter question, but this was considered beyond the scope of the present work.

The turbulent flux computations for H_T and E outlined in the foregoing subsection V.(C). and (D) represent minor modifications of the FNWC turbulent boundary layer model which has been appended to our radiation model (for the 2/3-CL case) for heat balance computational consistency tests, that is, to determine whether the net radiative flux at the surface is of the proper magnitude, relative to $E + H_T$.

VI. MERIDIONAL CROSS-SECTIONAL DEPICTION OF THE HEAT-BALANCE COMPUTATIONS

A. GENERAL

The general design of this section is to utilize all of the computational concepts discussed in Sections III, IV and V in the computations for a single time-step in the heating model developed for use in the FNWC prediction model. After testing F_2^* and ALB with the corresponding values of Raschke et al (1973), it was decided that only the computations by the 2/3-CL parameterization would be displayed in the meridional cross-sections (Figs. 6,7,8,9 and 10). The appropriate calculations were performed at each gridpoint of the four meridians used for presentation purposes in this section. However, the same type of computations using the full-CL parameterization were also made, but not presented in this section.

B. GEOGRAPHICAL REPRESENTATION OF THE HEAT-BALANCE DISTRIBUTION

The FNWC gridpoint processed analyses for 0000GMT, 16 April 1974 were used at the three Pacific cross-sections, while that for 1200GMT, 16 April 1974, were used for the single Atlantic meridian. This was done so that the set of gridpoints was considered to be subject to the actual radiative-transfer calculations involved for these specific times. Figure 6 depicts in symbolic language the key to

the computational entries in Fig. 7, 8, 9 and 10. This symbolic list presents the computations made at each radiative sounding gridpoint (I,J) having data in the form of Table I(b). The computations proceed from the top of the troposphere to the ocean surface and include the sensible and latent heat transfers, by the means of the computations of Section V. For purposes of climatological data comparison, Figs. 7, 8, 9 and 10 were developed by interpolating gridpoint results to integral multiples of 5-degree increments. The interpolation routine to this gridpoint spacing made use of the Lagrangian cubic interpolation scheme (after Spaeth, 1975).

$$\begin{aligned}
 Q(I) = & Q_1 \frac{(I-2)(I-3)(I-4)}{(1-2)(1-3)(1-4)} + Q_2 \frac{(I-1)(I-3)(I-4)}{(2-1)(2-3)(2-4)} \\
 & (6-1) \\
 & + Q_3 \frac{(I-1)(I-2)(I-4)}{(3-1)(3-2)(3-4)} + Q_4 \frac{(I-1)(I-2)(I-3)}{(4-1)(4-2)(4-3)}
 \end{aligned}$$

Finally for ease in reconciling the magnitudes of all heat-transfer rates, the time-dependent solar disposition rates have been averaged to 24-hourly rates.

C. EXPLANATION OF SYMBOLIC TERMS

1. Cross-Section at Level k=2 (Fig. 6)

The discussion of all insolation parameters discussed previously in Section IV dealt with the specific time of day that corresponded to the hour angle h for the instantaneous

time t under consideration. The incident solar insolation dealt with is then

$$F(S) = S \left(\frac{r}{r_m} \right)^{-2} \cos z \quad (6-2)$$

In order to avoid reference to specific map times t , the instantaneous solar hour-angles were $h = 35, 10, 55$, and 35 , respectively for cross-sections 1, 2, 3 and 4, as depicted in Figs. 7, 8, 9 and 10.

QAVE represents the 24-hour average of $F(2)$ and appears as the first input symbol in Fig. 6. Its value is considered to be more representative climatologically for the data day under consideration than $F(2)$.

QAVE is derived by the formula

$$QAVE = F(2) \frac{\overline{\overline{\cos z}}}{\cos z} \quad (6-3)$$

where

$$\overline{\overline{\cos z}} = [H \sin \phi \sin \delta + \cos \phi \cos \delta \sin H] / \pi \quad (6-4)$$

$$H = \arccos [-\tan \phi \tan \delta] \quad (6-5)$$

Here δ is the solar declination for 16 April 1974, and H is the hour angle at local sunset at latitude ϕ . $\overline{\overline{\cos z}}$ in (6-3) is equal to the 24-hour average cosine of the zenith angle, Eq. 4-2. The 24-hour time averaging period yielding QAVE gives heating results consistent in magnitude with the terrestrial flux divergences, which change only slightly with the time of day. The conversion to expected daily averaged solar disposition quantities is compatible with the determination of a heat budget for the given date (16 April 1974).

Other parameters needed for level $k=2$ are

$$QREF = REF(t) \left(\frac{\overline{\cos z}}{\cos z} \right) \quad (6-6)$$

where

$$REF(t) = F(2) - A26 - A610 - (IA10 + IS10) \quad (6-7)$$

$REF(t)$ is the instantaneous solar reflected insolation at a gridpoint and $QREF$ is its 24-hour average, assuming that planetary albedo remains constant for the 24-hour period, although it was calculated for the indicated solar time t . This assumption requires that the cloud amounts computed at the indicated synoptic times are representative of the entire day.

The same principle will be used with regard to all other solar parameters in the conversion from time-dependent values at solar time t to 24-hour averaged values. Superior bars ($\overline{}$) are not used in presenting the averaged values shown in the cross-sections key, Fig. 6. The 24-hour average system balance, $BALT$, is computed from

$$BALT = QAVE - (QREF + F_2^*) \quad (6-8)$$

for the tropopause level $k=2$ at the indicated latitude. Net terrestrial fluxes, such as F_2^* , were considered to be constant throughout the 24-hour period, a valid assumption if the cloud cover remains quasi-constant for the period.

2. Cross-Section in Layer (2,6)

The following definitions apply for the layer (2,6) as referred to in Fig. 6. All the heat transfers shown in this layer are assumed to be of radiative character only, as in the corresponding version of the FNWC heating model. The averaged radiative heating (cooling) rate is given by

$$\text{BAL26} = \text{Q26} - \text{F26} \quad (6-9)$$

where

$$\text{Q26} = \text{daily solar absorption in layer (2,6)}$$

and is defined relative to $\text{A26}(t)$ by a cosine transformation similar to Eq. 6-3, and

$$\text{F26} = \text{terrestrial cooling rate.}$$

3. Cross-Section in Layer (6,10)

The 24-hour average radiative cooling in the layer (6,10) is given by

$$\text{BAL610} = \text{Q610} - \text{F610} \quad (6-10)$$

where Q610 is the sum of Q68 and Q810 . BAL 68 has been taken as one-half of BAL610 . However, the heat balance in (8,10) has been modified for inclusion of H_T , as given by Eq. 5-7.

$$\text{BAL810} = \text{Q810} - \text{F810} + H_T = \text{BAL68} + H_T \quad (6-11)$$

Here H_T is the sensible heat flux convergence in the layer (8,10). F610 is the sum of F68 and F810 , the terrestrial flux losses for the respective layers.

4. Cross-Section at Air-Sea Interface (k=10)

The heat balance at the earth's surface (BALB) is as defined in the following equation

$$\text{BALB} = \text{QABG} - F_{10}^* - (H_T + E) \quad (6-12)$$

QABG is the 24-hour average insolation absorbed by the surface as

$$\text{QABG} = \text{QABG}(t) (\overline{\cos z} / \cos z) \quad (6-13)$$

H_T and E were computed respectively from Eqs. 5-7 and 5-13 and considered constant for the computational day, 16 April 1974.

D. LATITUDINAL CROSS-SECTIONS OF THE VERTICAL HEAT BALANCE FOR 16 APRIL 1974

Figs. 7, 8, 9 and 10 as previously explained represent the single time step of heating computations for each of the four meridians used in this study. The four figures have been divided into (a) tropical results and (b) mid-to-high-latitude results. While the results depicted in these cross-sections are exhibited as representing daily-averaged values, they are actually based upon heat-computations at the specific map times of 0000GMT and 1200GMT on 16 April 1974. Therefore, for these results to be meaningful as a stepwise part of the heat package subroutine of FNWC, the solar radiative absorption and reflectance terms would have to be

recoverable as a function of GMT, i.e.,

$$F(2,t) = QAVE* (\cos z / \overline{\overline{\cos z}}) \quad (6-14)$$

$$REF(t) = QREF* (\cos z / \overline{\overline{\cos z}}) \quad (6-15)$$

etc. Thus solar disposition terms may then be utilized in connection with the one-hour stepwise application of the thermodynamic equation of the set of primitive equations used in the FNWC prediction process, assuming the 2/3-CL parameterization.

The full-CL heat-balance cross-sections were also computed, but have not been presented here for the sake of brevity. However, certain key radiative heating (cooling) rates have been summarized in zonally-averaged form from both cloud parameterizations for the purposes of presenting the mean latitudinal comparisons (Section VII) of the purely radiative heat budget of the FNWC data as it was applicable to 16 April 1974.

k	LAT.	latitude of the gridpoints in 5° increments
	a) QAVE	24-hour averaged insolation at level k=2
	b) QREF	Reflected average insolation at level k=2
	c) F ₂ *	Net Outgoing long-wave flux at level k=2
2	d) BALT	averaged earth-tropospheric gain or loss (a-b-c)
	e) Q26	averaged solar insolation absorbed by layer (2,6), positive heating
	f) F26	IR flux loss by layer (2,6)
6	g) BAL26	averaged radiative cooling in layer (2,6) (e-f)
		- - - - -
	2/3 CL(1)	upper layer (4,6) cloud amount
	2/3 CL(2)	lower layer (8,9) cloud amount
		- - - - -
	h) Q68	averaged solar insolation absorbed by layer (6,8)
	i) F68	IR flux loss by layer (6,8)
	j) BAL68	averaged radiative cooling in layer (6,8) (h-i)
8	k) Q810	averaged solar insolation absorbed by layer (8,10)
	l) F810	IR flux loss by layer (8,10)
	m) H _T	sensible heat gain in layer (8,10)
	n) BAL810	averaged heat balance in layer (8,10) (k-l+m)
10		- - - - -
	o) QABG	averaged solar insolation absorbed by surface
	p) F ₁₀ *	net long-wave flux at earth's surface
	q) E+H _T	combined heat loss due to evaporation and sensible heat transport
	r) BALB	averaged warming or cooling at earth's surface (o-p-q)

Figure 6. Key to latitudinal cross-sections for Figs. 7,...,10. All radiative and turbulent transfer values are in ly min^{-1} for the levels or layers considered. The reduced cloud amounts 2/3 CL(1) and CL(2) are given by Eq. 2-5.

-20.0	-15.0	-10.0	-5.0	0.0	5.0	10.0	15.0	20.0	25.0
0.5169	0.5441	0.5671	0.5860	0.6005	0.6105	0.6160	0.6168	0.6132	0.6049
-0.2778	-0.2890	-0.2934	-0.3016	-0.2889	-0.2510	-0.2575	-0.2400	-0.1872	-0.1246
0.2710	0.2725	0.2811	0.2862	0.2933	0.3379	0.3442	0.3419	0.3630	0.3826
-0.0318	-0.0174	-0.0073	-0.0019	0.0181	0.0216	0.0143	0.0350	0.0631	0.0978
0.0583	0.0624	0.0639	0.0655	0.0654	0.0545	0.0517	0.0491	0.0404	0.0342
0.1332	0.1345	0.1326	0.1336	0.1298	0.1143	0.1135	0.1096	0.1006	0.1001
-0.0753	-0.0722	-0.0687	-0.0681	-0.0645	-0.0598	-0.0618	-0.0606	-0.0601	-0.0661
0.596	0.605	0.559	0.540	0.498	0.232	0.187	0.171	0.039	0.0
0.754	0.736	0.718	0.731	0.622	0.544	0.600	0.513	0.339	0.067
0.0260	0.0269	0.0289	0.0308	0.0308	0.0354	0.0384	0.0365	0.0339	0.0262
0.0341	0.0382	0.0421	0.0460	0.0493	0.0683	0.0722	0.0696	0.0790	0.0732
-0.0083	-0.0113	-0.0131	-0.0153	-0.0185	-0.0330	-0.0338	-0.0330	-0.0451	-0.0470
0.0260	0.0269	0.0289	0.0308	0.0308	0.0354	0.0384	0.0365	0.0339	0.0262
0.0341	0.0382	0.0421	0.0460	0.0493	0.0683	0.0722	0.0696	0.0790	0.0732
0.0299	0.0229	0.0166	0.0084	-0.0012	0.0094	0.0273	0.0187	-0.0102	-0.0154
0.0219	0.0116	0.0035	-0.0068	-0.0197	-0.0235	-0.0065	-0.0144	-0.0554	-0.0624
0.1292	0.1390	0.1519	0.1574	0.1844	0.2344	0.2300	0.2548	0.3179	0.3939
0.0692	0.0615	0.0642	0.0606	0.0649	0.0871	0.0862	0.0931	0.1044	0.1359
0.2328	0.1864	0.1888	0.1381	0.0889	0.1640	0.2293	0.2052	0.0448	0.0379
-0.1729	-0.1091	-0.1012	-0.0413	0.0307	-0.0167	-0.0856	-0.0437	0.1686	0.2201

Figure 7(a). 125.0 Longitudinal cross-section, tropical section. Refer to Fig.6 for key. Values computed from data for 16 april 1974 for 2/3-CL case only.

30.0 35.0 40.0 45.0 50.0 55.0

0.5923	0.5752	0.5540	0.5288	0.4999	0.4675
-0.1113	-0.1155	-0.1188	-0.1790	-0.2197	-0.1082
0.3888	0.4034	0.3910	0.3638	0.3323	0.3700
0.0923	0.0564	0.0444	-0.0140	-0.0521	-0.0107
0.0288	0.0188	0.0167	0.0114	0.0226	0.0211
0.0942	0.0748	0.0743	0.0566	0.0908	0.0739
-0.0655	-0.0560	-0.0576	-0.0452	-0.0582	-0.0528
0.0	0.0	0.0	0.0	0.0	0.0
0.0	0.0	0.007	0.375	0.648	0.0
0.0239	0.0180	0.0190	0.0360	0.0329	0.0140
0.0786	0.0834	0.0786	0.0996	0.0866	0.0476
-0.0546	-0.0654	-0.0597	-0.0634	-0.0537	-0.0337
0.0239	0.0180	0.0190	0.0360	0.0329	0.0140
0.0786	0.0834	0.0786	0.0996	0.0866	0.0476
-0.0250	-0.0191	-0.0008	0.0559	0.0323	0.0772
-0.0796	-0.0844	-0.0605	-0.0076	-0.0513	0.0435
0.4043	0.4050	0.3807	0.2664	0.1918	0.3102
0.1373	0.1617	0.1594	0.1083	0.0585	0.2008
0.0017	0.0574	0.0960	0.2102	0.0361	0.4516
0.2653	0.1859	0.1253	-0.0520	0.0373	-0.3421

Figure 7(b). 125^W Longitudinal cross-section, higher latitude section. Refer to

Fig. 6 for key. Values computed from data for 16 April 1974.

0.0	5.0	10.0	15.0	20.0	25.0
0.6005	0.6105	0.6160	0.6169	0.6132	0.6049
-.2196	-.2178	-.2168	-.2348	-.2251	-.1906
0.3402	0.3634	0.3858	0.3914	0.3865	0.3580
0.0406	0.0293	0.0134	-.0093	0.0016	0.0563
0.0493	0.0435	0.0369	0.0333	0.0327	0.0377
0.1157	0.1098	0.1038	0.1064	0.1067	0.1076
-.0664	-.0663	-.0668	-.0731	-.0740	-.0699
0.237	0.114	0.0	0.0	0.0	0.074
0.490	0.543	0.588	0.633	0.609	0.447
0.0326	0.0369	0.0401	0.0386	0.0393	0.0325
0.0707	0.0845	0.0972	0.0970	0.0949	0.0730
-.0380	-.0477	-.0571	-.0585	-.0557	-.0404
0.0326	0.0369	0.0401	0.0386	0.0393	0.0325
0.0707	0.0845	0.0972	0.0970	0.0949	0.0730
-.0088	-.0053	0.0033	0.0325	0.0216	0.0245
-.0469	-.0529	-.0538	-.0259	-.0341	-.0159
0.2662	0.2755	0.2820	0.2717	0.2769	0.3116
0.0832	0.0844	0.0877	0.0909	0.0900	0.1045
0.0582	0.0736	0.1053	0.2986	0.2074	0.2196
0.1250	0.1175	0.0889	-.1179	-.0205	-.0126

Figure 8(a). 170W longitudinal cross-section, tropical section. Refer to Fig. 6 for key. Values computed from data for 16 April 1974.

30.0	35.0	40.0	45.0	50.0	55.0	60.0	65.0
0.5923	0.5752	0.5540	0.5288	0.4999	0.4675	0.4322	0.3944
-0.1438	-0.0964	-0.1270	-0.1939	-0.2376	-0.2249	-0.2244	-0.1947
0.3436	0.3683	0.3221	0.3143	0.2858	0.2904	0.2752	0.2085
0.1048	0.1105	0.1050	0.0205	-0.0236	-0.0477	-0.0675	-0.0089
0.0368	0.0270	0.0314	0.0255	0.0241	0.0186	0.0178	0.0317
0.1033	0.0970	0.0950	0.0968	0.0977	0.0871	0.0794	0.0949
-0.0666	-0.0700	-0.0635	-0.0714	-0.0735	-0.0685	-0.0616	-0.0633
0.108	0.0	0.162	0.066	0.118	0.025	0.069	0.531
0.238	0.137	0.151	0.560	0.791	0.820	0.880	0.565
0.0251	0.0228	0.0189	0.0309	0.0312	0.0313	0.0284	0.0125
0.0616	0.0732	0.0562	0.0747	0.0674	0.0651	0.0684	0.0160
-0.0365	-0.0504	-0.0373	-0.0437	-0.0362	-0.0339	-0.0400	-0.0036
0.0251	0.0228	0.0189	0.0309	0.0312	0.0313	0.0284	0.0125
0.0616	0.0732	0.0562	0.0747	0.0674	0.0651	0.0684	0.0160
0.0007	-0.0141	-0.0082	-0.0035	0.0215	0.0783	0.0770	0.0753
-0.0358	-0.0646	-0.0454	-0.0472	-0.0147	0.00445	0.0370	0.0719
0.3613	0.4063	0.3578	0.2476	0.1757	0.1614	0.1331	0.1430
0.1170	0.1249	0.1146	0.0683	0.0534	0.0730	0.0590	0.0816
0.1065	0.0285	0.0416	0.0206	0.0692	0.1488	0.1329	0.1314
0.1378	0.2530	0.2014	0.1587	0.0531	-0.0604	-0.0587	-0.0700

Figure 8(b). 170W longitudinal cross-section, higher latitude section. Refer to Fig.6 for key. Values computed from data for 16 April 1974.

-5.0	0.0	5.0	10.0	15.0	20.0	25.0
0.5857	0.6005	0.6105	0.6160	0.6168	0.6132	0.6049
-.2341	-.1595	-.2059	-.2276	-.2192	-.2411	-.2766
0.3316	0.3984	0.3946	0.4202	0.4184	0.3857	0.3809
0.0199	0.0426	0.0101	-.0319	-.0207	-.0136	-.0525
0.0558	0.0421	0.0424	0.0319	0.0318	0.0411	0.0383
0.1238	0.1120	0.1147	0.1214	0.1288	0.1152	0.1154
-.0685	-.0698	-.0723	-.0895	-.0970	-.0740	-.0771
0.283	0.014	0.009	0.0	0.0	0.015	0.0
0.532	0.380	0.568	0.645	0.608	0.683	0.829
0.0357	0.0393	0.0450	0.0503	0.0485	0.0436	0.0446
0.0695	0.0942	0.1031	0.1102	0.0994	0.1032	0.1092
-.0338	-.0550	-.0581	-.0598	-.0509	-.0595	-.0645
0.0357	0.0393	0.0450	0.0503	0.0485	0.0436	0.0446
0.0695	0.0942	0.1031	0.1102	0.0994	0.1032	0.1092
-.0437	-.0137	-.0180	0.0047	0.0228	-.0119	-.0069
-.0777	-.0685	-.0761	-.0552	-.0281	-.0714	-.0714
0.2241	0.3204	0.2723	0.2559	0.2689	0.2438	0.2009
0.0682	0.0980	0.0758	0.0786	0.0906	0.0643	0.0473
-.1928	0.0453	-.0243	0.1205	0.2603	0.0049	0.0256
0.3496	0.1771	0.2228	0.0570	-.0821	0.1745	0.1280

Figure 9(a). 145E Longitudinal cross-section, tropical section. Refer to Fig. 6 for key. Values computed from data for 16 April 1974.

30.0	35.0	40.0	45.0	50.0	55.0
0.5923	0.5752	0.5540	0.5288	0.4999	0.4675
-0.2993	-0.3365	-0.2838	-0.2192	-0.2672	-0.2364
0.3084	0.2302	0.2285	0.1823	0.2185	0.1926
-0.0155	0.0086	0.0418	0.1273	0.0141	0.0386
0.0528	0.0679	0.0565	0.0577	0.0395	0.0422
0.1272	0.1357	0.1208	0.1009	0.1021	0.0984
-0.0743	-0.0678	-0.0643	-0.0432	-0.0625	-0.0563
0.316	0.718	0.601	0.762	0.546	0.623
0.847	0.955	0.707	0.037	0.707	0.528
0.0360	0.0275	0.0226	0.0085	0.0200	0.0149
0.0770	0.0251	0.0283	0.0098	0.0338	0.0180
-0.0410	0.0025	-0.0057	-0.0012	-0.0138	-0.0031
0.0360	0.0275	0.0226	0.0085	0.0200	0.0149
0.0770	0.0251	0.0283	0.0098	0.0338	0.0180
-0.0272	0.0012	0.0279	-0.0174	0.0122	0.0073
-0.0682	0.00638	0.0221	-0.0187	-0.0017	0.0042
0.1680	0.1156	0.1686	0.2348	0.1531	0.1594
0.0272	0.0444	0.0510	0.0618	0.0488	0.0582
-0.0901	0.1883	0.1022	-0.0033	0.0395	0.0352
0.2309	-0.1170	0.0153	0.1765	0.0648	0.0659

Figure 9(b). 145E Longitudinal cross-section, higher latitude section. Refer to

Fig. 6 for key. Values computed from data for 16 April 1974.

-20.0	-15.0	-10.0	-5.0	0.0	5.0	10.0	15.0	20.0	25.0
0.5169	0.5441	0.5671	0.5860	0.6005	0.6105	0.6160	0.6168	0.6132	0.6049
-0.2312	-0.2343	-0.1999	-0.2123	-0.2323	-0.2086	-0.1623	-0.1616	-0.1919	-0.1991
0.2994	0.3160	0.3595	0.3402	0.3282	0.3497	0.3701	0.3702	0.3908	0.4052
-0.0140	-0.0063	0.0077	0.0334	0.0400	0.0522	0.0836	0.0851	0.0304	0.0007
0.0535	0.0535	0.0461	0.0527	0.0565	0.0505	0.0436	0.0409	0.0315	0.0203
0.1284	0.1266	0.1173	0.1236	0.1252	0.1160	0.1062	0.1037	0.1039	0.0853
-0.0747	-0.0731	-0.0712	-0.0708	-0.0688	-0.0655	-0.0626	-0.0629	-0.0725	-0.0650
0.471	0.390	0.161	0.278	0.329	0.196	0.071	0.045	0.0	0.0
0.570	0.580	0.505	0.448	0.488	0.448	0.323	0.336	0.490	0.509
0.0257	0.0294	0.0356	0.0320	0.0326	0.0348	0.0341	0.0347	0.0412	0.0423
0.0466	0.0587	0.0822	0.0691	0.0687	0.0790	0.0856	0.0869	0.1033	0.1159
-0.0210	-0.0293	-0.0465	-0.0372	-0.0359	-0.0443	-0.0514	-0.0522	-0.0620	-0.0736
0.0257	0.0294	0.0356	0.0320	0.0326	0.0348	0.0341	0.0347	0.0412	0.0423
0.0466	0.0587	0.0822	0.0691	0.0687	0.0790	0.0856	0.0869	0.1033	0.1159
0.0090	-0.0040	-0.0168	-0.0173	-0.0207	-0.0241	-0.0285	-0.0259	-0.0168	-0.0038
-0.0122	-0.0333	-0.0633	-0.0544	-0.0567	-0.0684	-0.0799	-0.0782	-0.0788	-0.0775
0.1806	0.1974	0.2499	0.2569	0.2464	0.2818	0.3417	0.3453	0.3073	0.3009
0.0779	0.0720	0.0779	0.0783	0.0656	0.0756	0.0926	0.0928	0.0803	0.0879
0.1710	0.0240	-0.0257	0.0045	-0.0202	-0.0712	-0.1133	-0.0610	0.0007	0.0564
-0.0682	0.1014	0.1978	0.1740	0.2010	0.2775	0.3623	0.3135	0.2264	0.1566

Figure 10(a). 35W Longitudinal cross-section, tropical section. Refer to Fig. 6 for key. Values computed from data for 16 April 1974.

30.0	35.0	40.0	45.0	50.0	55.0	60.0
0.5923	0.5752	0.5540	0.5288	0.4999	0.4675	0.4321
-1.802	-2.082	-1.884	-1.477	-1.394	-1.772	-2.194
0.3749	0.3474	0.3409	0.3441	0.3207	0.2642	0.2309
0.0371	0.0197	0.0247	0.0369	0.0397	0.0250	-0.0180
0.0281	0.0263	0.0206	0.0153	0.0217	0.0331	0.0398
0.0954	0.0917	0.0854	0.0728	0.0386	0.1027	0.1119
-0.0573	-0.0654	-0.0648	-0.0575	-0.0669	-0.0695	-0.0721
0.0	0.0	0.0	0.0	0.060	0.389	0.584
0.437	0.568	0.504	0.340	0.252	0.250	0.572
0.0320	0.0330	0.0288	0.0243	0.0195	0.0152	0.0175
0.0844	0.0704	0.0580	0.0558	0.0425	0.0303	0.0352
-0.0523	-0.0373	-0.0291	-0.0314	-0.0230	-0.0151	-0.0177
0.0320	0.0330	0.0238	0.0243	0.0195	0.0152	0.0175
0.0844	0.0704	0.0580	0.0558	0.0425	0.0303	0.0352
0.0194	0.0933	0.1982	0.2483	0.1672	0.0426	-0.0103
-0.0330	0.0560	0.1691	0.2168	0.1442	0.0274	-0.0280
0.3199	0.2747	0.2873	0.3170	0.2996	0.2267	0.1381
0.1107	0.1150	0.1396	0.1598	0.1472	0.1008	0.0486
0.1576	0.3252	0.5011	0.5590	0.3825	0.1472	-0.0045
0.0516	-0.1655	-0.3534	-0.4018	-0.2300	-0.0213	0.0940

Figure 10(b). 35W Longitudinal cross-section, higher latitude section. Refer to

Fig. 6 for key. Values computed from data for 16 April 1974.

VII. THE LATITUDINAL DISTRIBUTION OF
RADIATIONAL BALANCE TERMS OF THE
OCEAN-ATMOSPHERE SYSTEM

A. GENERAL

The latitudinally-distributed results of the purely radiative contributions, over the ocean-atmosphere system, are presented in Figs. 12(a,b) for the 2/3-CL and 13(a,b) for the full-CL cases respectively. These cross-sections show the results after averaging over the four meridians considered in this study. The results are displayed in the format of Fig. 11. Radiative transfer Q68 and Q810 have been combined with F68 and F810 of Fig. 6 to compute layer-average radiational warming rates in the layer (6,10). The turbulent transfer heating rates $E + H_T$ into the atmosphere (and the corresponding cooling rates in the ocean) which were included in the results of Figs. 7, 8, 9 and 10 are now omitted in the radiative composites presented in Figs. 12 and 13.

In obtaining latitudinally-distributed means of radiative heating rates at each five-degree multiple of latitude ϕ , all values of each radiative parameter listed in Fig. 11 at latitude ϕ in the range 20S,...,65N (5-degree increments) were simply averaged over the four meridians providing the averaged value at ϕ . At $\phi = 65N$ there was only one contribution to the latitudinal average, while in the Southern

Hemisphere latitudes, 20S, 15 and 10S, only two values (on $\lambda = 125W$ and $\lambda = 35W$) of each parameter contributed to the means listed in Figs. 12 and 13. At 5S, there were three sets of radiative parameters entering into $\overline{Q(\phi)}$. Otherwise, there were four values of each radiative parameter entering into the computed radiative mean values $\overline{Q(\phi)}$ of the cross-sections. Therefore, near the northern and southern boundaries of Figs. 12 and 13, the listed values may not be equally representative, although the general trend should be reliable. Fig. 14, using data extracted from Figs. 12 and 13, tends to confirm this statement.

Figs. 12, 13 and 14 are also useful in determining the relative merits of the 2/3-CL model as compared to the full-CL model.

B. EARTH-TROPOSPHERE SYSTEM RADIATIONAL BALANCE SUMMARY

The latitudinally-averaged distributions of the three key radiative parameters, R_s , R_a and R as functions of latitude for both the 2/3-CL and full-CL cases are shown in Fig. 14. The radiative-balance parameters were defined (after Malkus, 1962) as $R_s(\phi)$, the mean radiative-energy transfer rate across the top of the ocean-tropospheric system at $k=2$ (referred to as BALT in Fig. 11); $R_a(\phi)$, the mean radiative cooling rate in the troposphere (BAL26 + BAL610 in Fig. 11); and $R(\phi)$, the mean radiative warming (cooling) rate at the earth's surface (BAL10 in Fig. 11).

k	LAT	latitude of the gridpoints in 5° increments
a)	QAVE	24-hour averaged mean insolation at level k=2
b)	QREF	mean reflected average insolation at level k=2
c)	F ₂ *	mean net outgoing long-wave flux at level k=2
d)	B ₂ LT	mean averaged earth tropospheric gain rate (a-b-c)
2		
e)	Q26	mean averaged solar insolation absorbed by layer (2,6)
f)	F26	mean IR flux loss by layer (2,6)
g)	BAL26	mean averaged radiative cooling rate, layer (2,6) (e-f)
-	-	-
	(CL ₁)	upper layer (4,6) cloud amount
	(CL ₂)	lower layer (8,9) cloud amount
6		
-	-	-
h)	Q610	mean averaged solar insolation absorbed by layer (6,10)
i)	F610	mean IR flux loss by layer (6,10)
j)	BAL610	mean averaged radiative cooling rate, layer (6,10) (h-i)
10		
k)	QABG	mean averaged solar insolation absorbed by surface
l)	F ₁₀ *	mean net long-wave flux at earth's surface
m)	BAL10 = QABG-F ₁₀ *	mean averaged radiational warming (cooling) rate at earth's surface

Figure 11. Key to zonally-averaged radiational cross-section for Figs. 12(a,b) and 13(a,b). All radiational values have been averaged over a 24-hour day and are expressed in ly min^{-1} for the levels or layers considered. The zonal averages have been taken over the meridians (125°W, 170°W, 145°E and 35°W) used in this study. The cloud-amounts (in parentheses) are by the 2/3-CL model in Fig. 12 and by the full-CL model in Fig. 13.

-20.0	-15.0	-10.0	-5.0	0.0	5.0	10.0	15.0	20.0	25.0
0.5169	0.5441	0.5671	0.5859	0.6005	0.6105	0.6160	0.6168	0.6132	0.6049
-0.2545	-0.2616	-0.2466	-0.2493	-0.2251	-0.2208	-0.2161	-0.2139	-0.2113	-0.1977
0.2852	0.2942	0.3203	0.3194	0.3400	0.3614	0.3801	0.3804	0.3815	0.3817
-0.0229	-0.0119	0.0002	0.0171	0.0353	0.0283	0.0198	0.0225	0.0204	0.0256
0.0559	0.0579	0.0550	0.0580	0.0553	0.0477	0.0410	0.0388	0.0364	0.0326
0.1308	0.1306	0.1249	0.1270	0.1207	0.1137	0.1112	0.1122	0.1066	0.1021
-0.0750	-0.0727	-0.0700	-0.0691	-0.0674	-0.0660	-0.0702	-0.0734	-0.0702	-0.0695
0.534	0.497	0.360	0.367	0.269	0.138	0.065	0.054	0.013	0.018
0.662	0.658	0.612	0.570	0.495	0.525	0.539	0.522	0.530	0.463
0.0516	0.0563	0.0646	0.0656	0.0677	0.0760	0.0815	0.0791	0.0790	0.0728
0.0807	0.0969	0.1243	0.1231	0.1415	0.1674	0.1826	0.1764	0.1902	0.1857
-0.0291	-0.0406	-0.0597	-0.0574	-0.0738	-0.0914	-0.1011	-0.0973	-0.1112	-0.1128
0.1549	0.1682	0.2009	0.2128	0.2543	0.2660	0.2774	0.2852	0.2865	0.3018
0.0736	0.0667	0.0710	0.0690	0.0779	0.0802	0.0863	0.0919	0.0847	0.0939
0.0813	0.1014	0.1299	0.1437	0.1764	0.1858	0.1911	0.1933	0.2017	0.2079

Figure 12(a). Zonally-averaged radiational cross-section for tropical latitudes with 2/3-CL model. Refer to Fig. 11 for key. All values listed are daily averages in ly min^{-1} and are computed from data for 16 April 1974.

30.0	35.0	40.0	45.0	50.0	55.0	60.0	65.0
0.5925	0.5752	0.5540	0.5288	0.4999	0.4675	0.4321	0.3944
-0.1837	-0.1892	-0.1795	-0.1849	-0.2160	-0.1867	-0.2219	-0.1947
0.3539	0.3373	0.3206	0.3011	0.2893	0.2793	0.2530	0.2085
0.0547	0.0488	0.0540	0.0427	-0.0055	0.0016	-0.0428	-0.0089
0.0366	0.0350	0.0313	0.0275	0.0270	0.0288	0.0288	0.0317
0.1050	0.0938	0.0939	0.0818	0.0948	0.0905	0.0957	0.0949
-0.0684	-0.0648	-0.0626	-0.0543	-0.0678	-0.0618	-0.0669	-0.0633
0.106	0.179	0.191	0.207	0.181	0.259	0.327	0.531
0.380	0.415	0.342	0.328	0.602	0.400	0.726	0.565
0.0585	0.0507	0.0447	0.0499	0.0518	0.0377	0.0459	0.0250
0.1508	0.1260	0.1106	0.1200	0.1152	0.0805	0.1036	0.0319
-0.0923	-0.0754	-0.0659	-0.0701	-0.0634	-0.0428	-0.0578	-0.0069
0.3134	0.3004	0.2986	0.2665	0.2051	0.2144	0.1356	0.1430
0.0981	0.1115	0.1162	0.0995	0.0795	0.1082	0.0538	0.0816
0.2153	0.1889	0.1824	0.1669	0.1256	0.1062	0.0818	0.0614

Figure 12(b). Zonally-averaged radiational cross-section for higher latitudes

with 2/3-CL model. Refer to Fig. 11 for key. All values listed are daily averages in ly min^{-1} and are from data for 16 April 1974.

-20.0	-15.0	-10.0	-5.0	0.0	5.0	10.0	15.0	20.0	25.0
0.5169	0.5441	0.5671	0.5859	0.6005	0.6105	0.6160	0.6168	0.6132	0.6049
-0.3057	-0.3170	-0.3023	-0.3106	-0.2843	-0.2848	-0.2813	-0.2790	-0.2748	-0.2408
0.2581	0.2638	0.3005	0.2947	0.3241	0.3499	0.3711	0.3714	0.3752	0.3768
-0.0469	-0.0418	-0.0358	-0.0235	-0.0079	-0.0243	-0.0364	-0.0335	-0.0368	-0.0126
0.0014	0.0633	0.0592	0.0624	0.0568	0.0498	0.0422	0.0397	0.0368	0.0330
0.1588	0.1567	0.1442	0.1466	0.1349	0.1212	0.1149	0.1152	0.1075	0.1032
-0.0973	-0.0933	-0.0851	-0.0840	-0.0781	-0.0715	-0.0728	-0.0755	-0.0707	-0.0702
0.801	0.746	0.541	0.551	0.404	0.207	0.097	0.081	0.020	0.028
0.926	0.933	0.878	0.821	0.740	0.785	0.804	0.781	0.784	0.632
0.0471	0.0530	0.0648	0.0660	0.0709	0.0843	0.0923	0.0902	0.0910	0.0805
0.0481	0.0695	0.1112	0.1101	0.1383	0.1798	0.2019	0.1951	0.2139	0.1999
-0.0009	-0.0166	-0.0464	-0.0442	-0.0674	-0.0956	-0.1096	-0.1050	-0.1230	-0.1194
0.1026	0.1107	0.1409	0.1471	0.1884	0.1916	0.2002	0.2079	0.2106	0.2506
0.0512	0.0426	0.0452	0.0422	0.0508	0.0488	0.0542	0.0609	0.0537	0.0737
0.0514	0.0681	0.0957	0.1049	0.1376	0.1428	0.1460	0.1470	0.1569	0.1759

Figure 13(a). Similar to Fig. 12(a) except full-CL model (after Smagorinsky, Eq. 2-4) is used in all radiative calculations.

30.0	35.0	40.0	45.0	50.0	55.0	60.0	65.0
0.5923	0.5752	0.5540	0.5288	0.4999	0.4675	0.4321	0.3944
-0.2167	-0.2161	-0.2145	-0.2278	-0.2597	-0.2157	-0.2543	-0.2502
0.3463	0.3290	0.3099	0.2914	0.2763	0.2665	0.2369	0.1315
0.0293	0.0301	0.0296	0.0096	-0.0362	-0.0146	-0.0591	-0.0374
0.0382	0.0369	0.0338	0.0294	0.0295	0.0319	0.0324	0.0377
0.1104	0.1062	0.1015	0.0864	0.1024	0.1006	0.1086	0.1202
-0.0722	-0.0693	-0.0677	-0.0570	-0.0729	-0.0687	-0.0763	-0.0825
0.161	0.248	0.277	0.270	0.270	0.386	0.490	0.796
0.502	0.513	0.483	0.493	0.832	0.543	0.926	0.977
0.0617	0.0522	0.0476	0.0575	0.0581	0.0392	0.0466	0.0293
0.1517	0.1212	0.1052	0.1253	0.1165	0.0702	0.0898	0.0047
-0.0900	-0.0690	-0.0576	-0.0678	-0.0585	-0.0310	-0.0432	0.0245
0.2757	0.2700	0.2581	0.2141	0.1526	0.1807	0.0989	0.0772
0.0842	0.1016	0.1032	0.0798	0.0574	0.0957	0.0386	0.0566
0.1914	0.1684	0.1549	0.1343	0.0952	0.0850	0.0603	0.0206

Figure 13(b). Similar to Fig. 12(b) except full-CL model (after Smagorinsky, Eq. 2-4) is used in all radiative calculations.

The relationship between these radiative parameters is

$$R_s = R_a + R \quad (7-1)$$

Tables X, XI and XII list the zonally-averaged values of R_s , R and R_a as a function of latitude ϕ for the 2/3-CL and the full-CL cases. Weighted averages for any Q -value are then computed using the following cosine weighting scheme (Eq. 7-2, Spaeth, 1975).

$$Q_{\text{wt. avg.}} = \frac{\sum_{i=1}^{18} \frac{k_i}{4} \left(\sum_{j=1}^4 \frac{Q_{ji}}{k_i} \right) \cos \phi_i}{\sum_{i=1}^{18} \frac{k_i}{4} \cos \phi_i} \quad (7-2)$$

where Q_{ji} = value on meridian j at latitude ϕ_i and k_i is the number $k=1, \dots, 4$ of meridional observations available for the meridional averages at ϕ_i . Note that $i=1, \dots, 18$ corresponds to the 18 latitudes, $\phi_i = 20, \dots, 65$ latitude degrees. Tables X, XI and XII depict comparative values of R_s , R and R_a by latitudes for both 2/3-CL and full-CL parameterizations for 16 January, 16 April and 16 July 1974.

In Fig. 14, the dominant net-flux terms across interfaces are $R_s(\phi)$ and $R(\phi)$. The net flux values obtained from the 2/3-CL model (denoted R_{s1}) exceeded those by the full-CL model (R_{s2}) at all latitudes. Both R_s functions had maxima at 30N on 16 April 1974. Comparative values of the mean

latitudinal distributions of the radiative balance $R(\phi)$ at sea level for the 2/3-CL and full-CL cases were also extracted from Figs. 12 and 13. They were tabulated in the center portion of Tables X, XI and XII for 16 April 1974 and plotted also as a function of latitude in Fig. 14. It is to be noted that the 2/3-CL case (denoted R_1) is greater than R_2 over the entire range of latitude under consideration in Fig. 14. The difference $R_1 - R_{s1}$ is very nearly equal to that of $R_2 - R_{s2}$, so that the net cooling in air, $R_{a1} \doteq R_{a2}$ over the entire range of latitude in Fig. 14.

In summary, for 16 April 1974, Table X and Fig. 14 show that a substantial positive difference in net flux exists at the troposphere $k=2$ for the case of R_{s1} (for 2/3-CL) over the case of R_{s2} (for full-CL). The zonally-averaged R_s -difference for the range of latitudes in Spring is $.0380 \text{ cal cm}^{-2} \text{ min}^{-1}$. Likewise, Table XI and Fig. 14 show that the net flux at the surface for the 2/3-CL exceeds the full-CL by $.0351 \text{ cal cm}^{-2} \text{ min}^{-1}$, when both sets of values R_1 and R_2 have been meridionally-averaged. However, the difference $R_{a1} - R_{a2}$ is negligible regardless of whether 2/3-CL or full-CL parameterization was employed.

As contrasted with the Winter (16 January 1974) studied by Spaeth, no change in sign in $R_{s1} - R_{s2}$ and/or in $R_1 - R_2$ occurs for $\phi \geq 40\text{N}$. The reason for the consistent sign of the difference $R_{s1} - R_{s2} \doteq .03 \text{ cal cm}^{-2} \text{ min}^{-1}$ which exists at virtually all latitudes in April is that the "summerlike-effect" of an increase in effective insolation with decreased

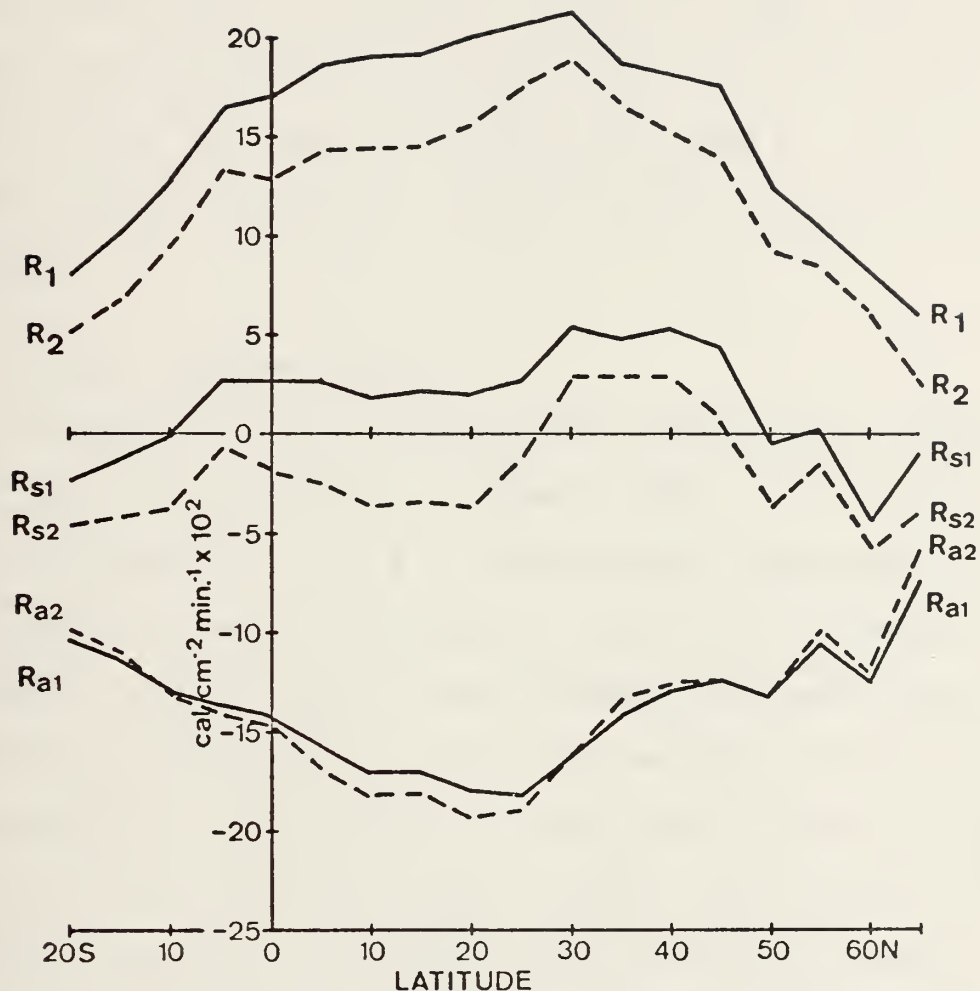


Figure 14. Radiational balance at the tropopause (R_s), at the ocean surface (R), and in the tropospheric column (R_a). Solid lines denote computations made with the 2/3-CL (subscripted "1") cloud model and dashed lines correspond to the full-CL model, (subscripted "2"). All computations are for 16 April 1974 in $\text{ly min}^{-1} \times 10^2$.

cloud-cover is dominant at all $\phi \leq 65\text{N}$ at this time of the year (when the declination is 8.5 degrees), whereas there is a smaller retention of IR net flux by the troposphere when the cloud-cover is reduced to 2/3-CL. These effects apply at all latitudes under study here, but undoubtedly, there could be a change of sign in both $R_{s1} - R_{s2}$ and $R_1 - R_2$ in latitudes further removed from the subsolar latitude for 16 April 1974.

C. CROSS-SEASONAL EFFECTS

Tables X, XI and XII show the cross-seasonal effects in R_s , R and R_a centered on 16 April 1974. It is clear that R_{s1} increases at each ϕ in the Northern Hemisphere in the time sequence 16 January through 16 July 1974. A similar effect applies to R_{s2} (full-CL case) through the same time sequence. Similar results apply to the time sequence for the sizable increases of net flux (R) at the earth's surface, both for the 2/3-CL and full-CL cases. These cross-seasonal results tend to confirm the validity of the radiative model.

In the Southern Hemisphere latitudes of Tables X, XI and XII, there is a systematic trend toward decreasing R_s -values in the time sequence 16 January through 16 July 1974. The same trend applies to R -values across the time sequence. Considering that this sequence corresponds to the periods of summer-fall-winter in the Southern Hemisphere, this cross-seasonal trend also appears to afford qualitative support to the radiational model tested here.

D. COMPARISON OF NET FLUX AT THE TOP OF THE MODEL ATMOSPHERE WITH SATELLITE OBSERVATIONS

Based upon observations of Raschke et al (1973) of $F2(RAS)$ and of the albedo $ALB(RAS)$ over the latitude-range of this study, the net flux parameter at the top of the atmosphere was defined for the NIMBUS III data-period (1-15 May 1969) by Raschke et al (1973), as

$$RN = QAVE * \frac{2.00}{1.92} (1-ALB(RAS)) - F2(RAS) \quad (7-3)$$

Raschke's computed values of the RN for this data period used a slightly different solar constant than that employed in this study ($S = 2.00 \text{ ly (min)}^{-1}$). Hence for purposes of consistency in comparisons, our average extraterrestrial insolation, $QAVE*(2.00/1.92)$ was used in the definition of RN in Eq. 7-3).

Values of RN were computed after Raschke at each five-degree latitude intersection on the four meridians where comparisons with the present model computations were possible. For the corresponding radiative model computations of this study, the following analog to Eq. 7-3 was adapted.

$$RNMOD = QAVE * \frac{2.00}{1.92} (1-ALBMOD) - FF2 \quad (7-4)$$

$FF2$ represents a parameter analogous to $F2(RAS)$, values of which were compared in Section III. E. on a latitudinal basis. Likewise, albedo values were compared on a latitudinal basis in Section IV. G.

The computational values of RNMOD for 16 April 1974 were computed using both the 2/3-CL and the full-CL cloud parameterizations. After obtaining averages across the four meridians, the latitudinal comparisons are depicted in Table XIII.

The first three columns of Table XIII show that the latitudinal distribution of RNMOD is somewhat smaller than the values of RN (after Raschke) at all latitudes except 55N. The difference

$$RN - RNMOD$$

is generally positive because of the consistently small albedos of the Raschke observations. This difference is considerably larger for the full-CL case, when the model albedo was recognized as being excessively high.

A comparison of the mean radiative balance R_s at the tropopause $k=2$ has been made with that at $k=0$, which has been denoted RNMOD. The results have been tabulated as a function of latitude in Table XIII. The R_s -values for the earth-troposphere have been extracted from Table X and appear in columns four and five of Table XIII. Recall that

$$R_s = QAVE (1-ALBMOD) - F_2^* . \quad (7-5)$$

In comparing Eqs. 7-4 and 7-5, it is clear that the incoming insolation used in the computation of R_s has been reduced by

4% of an amount which is approximately

$$\overline{QAVE - QREF} = .3602 \text{ ly (min)}^{-1} \quad (7-6)$$

averaged over all latitudes. However, $\overline{R_{s1}}$ exceeds $\overline{RNMOD(2/3)}$ by $.017 \text{ ly (min)}^{-1}$ which must therefore be accounted for by the fact

$$\overline{FF2 - F_2^*} = .023 - .006 + .04 \overline{(QAVE - QREF)} \quad (7-7)$$

for the 2/3-CL case. Approximately the same difference exists between comparisons for the full-CL cases.

The IR-flux divergence of (7-7) is due to the presence of water-vapor and CO_2 emitter masses operating in conformity with the F_2^* model (Eq. 3-5). These masses have not been subjected to compensating solar insolation absorption in the stratosphere, and the 4% solar absorption by oxygen and ozone is not sufficient to establish a stratospheric balance.

Lat.	Mid-Seasonal Dates					
	16 Jan 1974		16 April 1974		16 July 1974	
	R_{s1}	R_{s2}	R_{s1}	R_{s2}	R_{s1}	R_{s2}
20S	.0681	.0216	-.0229	-.0469	-.1012	-.1124
15	.0552	.0052	-.0119	-.0418	-.0817	-.1010
10	.0488	-.0039	.0002	-.0358	-.0546	-.0772
5	.0475	.0046	.0171	-.0235	-.0428	-.0616
0	.0182	-.0270	.0353	-.0079	.0132	-.0171
5	-.0050	-.0478	.0283	.0243	.0297	-.0062
10	-.0140	-.0428	.0198	-.0364	.0521	.0145
15	-.0489	-.0736	.0225	-.0335	.0635	.0211
20	-.0813	-.1010	.0204	-.0368	.0627	.0136
25	-.0938	-.1058	.0256	-.0126	.0825	.0380
30	-.0998	-.1041	.0547	.0293	.0945	.0560
35	-.1497	-.1551	.0488	.0301	.1018	.0607
40	-.1689	-.1706	.0540	.0296	.1254	.0888
45	-.1884	-.1835	.0427	.0096	.0884	.0612
50	-.2062	-.1969	-.0055	-.0362	.1461	.1038
55	-.1798	-.1671	.0016	-.0146	.1063	.0766
60	-.1932	-.1759	-.0428	-.0591	.1063	.1315
65N	-.2265	-.2265	-.0089	-.0374	.1990	.1640
<hr/>						
Wt. Avg.	-.1000	-.1139	.0227	-.0153	.0523	.0227

Table X. Cross-seasonal comparison of zonally-averaged values of R_s as a function of latitude. The averaged values for the 2/3-CL case are denoted with a subscripted 1 and the full-CL case values by a subscripted 2. (All values in $ly(min)^{-1}$).

Lat.	Mid-Seasonal Dates					
	16 Jan 1974		16 April 1974		16 July 1974	
	R ₁	R ₂	R ₁	R ₂	R ₁	R ₂
20S	.1622	.1123	.0813	.0514	.0598	.0546
15	.1624	.1125	.1015	.0681	.0954	.0852
10	.1780	.1310	.1299	.0957	.1276	.1134
5	.1902	.1537	.1438	.1049	.1375	.1224
0	.1802	.1443	.1164	.1376	.1732	.1486
5	.1697	.1387	.1858	.1294	.1773	.1463
10	.1645	.1454	.1911	.1460	.2041	.1726
15	.1374	.1226	.1933	.1470	.2216	.1866
20	.1123	.1022	.2018	.1569	.2373	.1987
25	.0807	.0738	.2079	.1769	.2579	.2225
30	.0475	.0429	.2153	.1915	.2616	.2285
35	.0152	.0145	.1889	.1684	.2774	.2429
40	-.0092	-.0072	.1824	.1549	.2927	.2605
45	-.0094	-.0068	.1670	.1343	.2364	.2102
50	-.0275	-.0200	.1256	.0952	.2747	.2309
55	-.0409	-.0300	.1062	.0850	.1816	.1438
60	-.0868	.0683	.0818	.0603	.2725	.2359
65N	-.0868	-.0868	.0614	.0206	.2637	.2154
<hr/>						
Wt.Avg.	.0668	.0581	.1684	.1333	.1879	.1349

Table XI. Cross-seasonal comparison of zonally-averaged values of R as a function of latitude ϕ . The averaged values for the 2/3-CL case are denoted with a subscripted 1 and the full-CL case values by a subscripted 2. (All values in $\text{ly} (\text{min})^{-1}$).

Lat.	Mid-Seasonal Dates					
	16 Jan 1974 R_{a1}	R_{a2}	16 April 1974 R_{a1}	R_{a2}	16 July 1974 R_{a1}	R_{a2}
20S	-.0942	-.0913	-.1042	-.0983	-.1611	-.1674
15	-.1073	-.1075	-.1134	-.1099	-.1772	-.1863
10	-.1292	-.1347	-.1297	-.1315	-.1824	-.1907
5	-.1426	-.1492	-.1267	-.1284	-.1804	-.1842
0	-.1621	-.1720	-.0811	-.0455	-.1603	-.1659
5	-.1746	-.1864	-.1575	-.1671	-.1476	-.1526
10	-.1787	-.1882	-.1713	-.1824	-.1521	-.1582
15	-.1863	-.1962	-.1708	-.1805	-.1582	-.1656
20	-.1937	-.2031	-.1814	-.1937	-.1748	-.1852
25	-.1745	-.1796	-.1823	-.1895	-.1756	-.1847
30	-.1472	-.1471	-.1606	-.1622	-.1672	-.1727
35	-.1648	-.1696	-.1401	-.1383	-.1757	-.1824
40	-.1597	-.1634	-.1284	-.1253	-.1657	-.1718
45	-.1791	-.1768	-.1243	-.1247	-.1482	-.1491
50	-.1788	-.1769	-.1311	-.1314	-.1286	-.1274
55	-.1065	-.1371	-.1046	-.0996	-.0754	-.0675
60	-.1397	-.1077	-.1246	-.1194	-.1123	-.1045
65N	-.1668	-.1397	-.0703	-.0580	-.0650	-.0517
Wt.Avg.	-.1668	-.1720	-.1457	-.1486	-.1626	-.1577

Table XII. Cross-seasonal comparison of the zonally-averaged values of R_a as a function of latitude ϕ . The averaged values for the ^a2/3-CL case are denoted with a subscripted 1 and the full-CL case values by a subscripted 2. (All values in $1y \text{ (min)}^{-1}$).

Lat.	RNM0D		Ocean-Troposphere		RNRAS
	2/3-CL	Full-CL	R_{s1}	R_{s2}	
20S	-.0523	-.0762	-.0229	-.0469	.0369
15	-.0394	-.0700	-.0119	-.0418	.0554
10	-.0227	-.0588	.0002	-.0358	.0745
5	.0076	-.0272	.0171	-.0235	.1083
0	.0093	-.0377	.0353	-.0079	.1304
5	.0134	-.0392	.0283	.0243	.1545
10	.0115	-.0448	.0198	-.0364	.1517
15	.0172	-.0390	.0225	-.0335	.1337
20	.0161	-.0412	.0204	-.0368	.1272
25	.0232	-.0150	.0256	-.0126	.1150
30	.0467	.0213	.0547	.0293	.1059
35	.0380	.0193	.0488	.0301	.0779
40	.0429	.0185	.0540	.0296	.0770
45	.0296	-.0036	.0427	.0096	.0570
50	-.0122	-.0430	-.0055	-.0362	.0251
55	-.0152	-.0314	.0016	-.0146	-.0216
60	-.0340	-.0505	-.0428	-.0591	-.0489
65N	-.0483	-.0770	-.0089	-.0374	-.0946
<hr/>					
Wt.Avg.	.0062	-.0328	.0227	-.0153	.0818

Table XIII. Comparison of the Ocean-Troposphere Net Radiation R_s at $k=2$, with the model computed Net Radiation at the top of the atmosphere RNM0D and with climatological Net Radiation at the top of the atmosphere from Raschke et al (1973) RNRAS. R_s and RNM0D have been computed using both the 2/3-CL and Full-CL parameterizations. R_{s1} is from 2/3-CL model and R_{s2} is from the full-CL model.

VIII. ZONALLY-AVERAGED TROPOSPHERIC
AND OCEANIC HEAT BUDGETS
FOR 16 APRIL 1974

A. THE TROPOSPHERIC HEAT BUDGET

By averaging over the tropospheric columns for the four meridians displayed in Figs. 7, 8, 9 and 10 latitude by latitude, the latitudinal distribution of $E + H_T$ results were obtained and are presented in Fig. 15. R_a , the tropospheric radiative net cooling is listed in Table XII. The zonally-averaged $E + H_T$ values computed from Eqs. 5-7 and 5-13 are displayed as a function of latitude in Table XIV. The resulting heating rate of the troposphere may then be expressed as a function of ϕ by the right side of Eq. 8-1,

$$Q_{va} + S_a = R_a + (E + H_T) . \quad (8-1)$$

Lat.	-20.	-15.	-10.	-5.	0.0	5.	10.	15.	20.
$E+H_T$.2019	.1059	.0815	.0167	.0430	.0355	.0855	.1758	.0645
Lat.	25.	30.	35.	40.	45.	50.	55.	60.	65.N
$E+H_T$.0849	.0439	.1499	.1852	.1966	.1318	.1957	.0642	.1314
Weighted Average = .1032									

Table XIV. Zonally-averaged values of $E+H_T$ as a function of latitude. (All values in $ly \text{ (min)}^{-1}$).

S_a is the storage heating rate of the column, and Q_{va} is the required flux-divergence of heat compatible with the heat balance equation for the column, for the observed values of

R_a , $E+H_\Gamma$ and S_a . Figure 15 depicts each quantity (R_a , $(E + H_\Gamma)$ and $(Q_{va} + S_a)$) as a function of latitude for the two cloud-model cases.

As noted in Section VII. B., $R_{a1} \doteq R_{a2}$ over the range of latitudes in this study, with little variation in R_a as a function of latitude. The distribution of $E + H_\Gamma$ as a function of latitude is independent of cloud-model. Therefore, Fig. 15 shows only one curve for $E + H_\Gamma$. The curves of $Q_{va} + S_a$ are also shown in Fig. 15, as the residual of the right sides of Eq. 8-1 for both the 2/3-CL and the full-CL cases, respectively. Note that $(Q_{va} + S_a)_1$ slightly exceeds $(Q_{va} + S_a)_2$ from 10S to 30N as a result of the corresponding excess of R_{a1} over R_{a2} for the same latitude range. Note that both $(Q_{va} + S_a)$ distributions reach maximum positive values at $\phi = 50N$, with a general positive trend from 35N to 55N. This feature follows from Eq. 8-1, since $(Q_{va} + S_a)$ must follow the trend of $(E + H_\Gamma)$ where the latitudinal variation of the latter function peaks more sharply, relative to the more or less uniform behavior of $R_a(\phi)$.

The cosine-weighted value of $\overline{Q_{va} + S_a} = -.0425 \text{ ly min}^{-1}$ per cm^2 column. $\overline{Q_{va}}$ has not been computed in this study; however, if the $\overline{Q_{va} + S_a}$ is attributed to mean storage-cooling $\overline{S_a}$ of the troposphere alone, the daily storage rate corresponds to a temperature-change rate given by

$$\left(\frac{\partial T}{\partial t}\right) = 4.1 \frac{\overline{R_a} + (\overline{E + H_\Gamma})}{\Delta P_{mb}} \times 1440 \text{ } ^\circ\text{C/day} \quad (8-2)$$

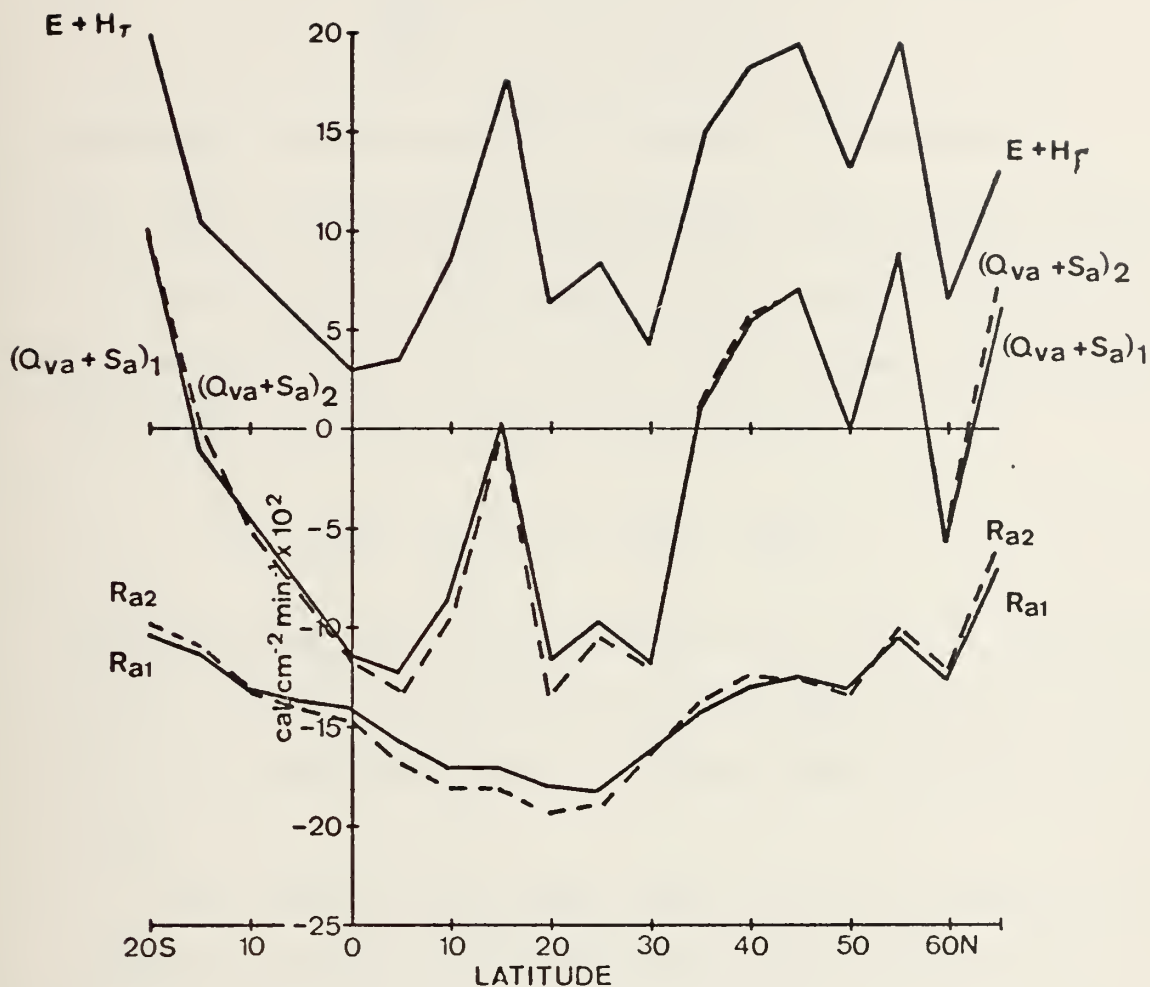


Figure 15. Distribution of R_a , $E+H_r$ and of $Q_{va}+S_a$ as a function of latitude for the two cloud-model cases. (solid curves represent the 2/3-CL case and dashed curves represent the full-CL case)

with $\Delta P \text{ mb} \doteq 800\text{mb}$ in the troposphere. The resultant cooling rate (8-2) over the tropospheric depth of 800mb, considering that zero lateral flux-divergence applies, is approximately

$$\overline{\left(\frac{\partial T}{\partial t}\right)} = -.31^{\circ}\text{C} (\text{day})^{-1}$$

averaged over the mean cm^2 tropospheric column.

B. THE LATITUDINALLY-AVERAGED HEAT BUDGET OF THE OCEAN

The latitudinally-averaged heat-budget of the ocean water-mass obeys the following thermodynamic relationship for both the 2/3-CL and full-CL cases.

$$Q_{vo} + S_o = R + -(E + H_T) \quad (8-3)$$

Note that Eq. 8-3 is the analog of Eq. 8-1 for the atmosphere, with $-(E + H_T)$ representing the average turbulent cooling rate for the water-mass by mixing across the sea-air interface.

The terms of the right side of Eq. 8-3 have been computed for each latitude and averaged zonally, with R and $E + H_T$ shown in Table XI and XIV, respectively. $Q_{vo} + S_o$ has been computed as the residual of these two terms as a function of latitude and the entire set of terms in Eq. 8-3 are graphed in Fig. 16 for both cloud cases.

The primary ocean-mass heating-function is R , the radiative heating rate at the ocean-air interface. As discussed in Section VII, $R_1 > R_2$ for all latitudes considered in this

study. Therefore, according to Eq. 8-3, $(Q_{vo} + S_o)_1$ must be greater than $(Q_{vo} + S_o)_2$ by the same amounts since $-(E + H_T)_1 = -(E + H_T)_2$. This means that the internal heating rate of the ocean-mass, as given in Eq. 8-3, is greater in the 2/3-CL case than in the full-CL case for all latitudes considered in this study. Q_{vo} is the required mean oceanic heat-flux divergence at latitude ϕ . Fig. 16 supports the conclusion of Von der Haar and Oort (1973) which requires increased lateral transport-divergences Q_{vo} in the oceans, based upon the recently observed satellite values of the global albedo. The values for $(Q_{vo} + S_o)$, from this study seem to corroborate the satellite findings.

The mean value of $\overline{(Q_{vo} + S_o)}_1$ computed between 20S-65N is

$$\overline{(Q_{vo} + S_o)}_1 = .0652 \text{ ly min}^{-1}$$

which corresponds to a mean heating rate in the water-mass column. It should be noted that this heating rate is noticeably larger, and of opposite sign, than the corresponding atmospheric effect.

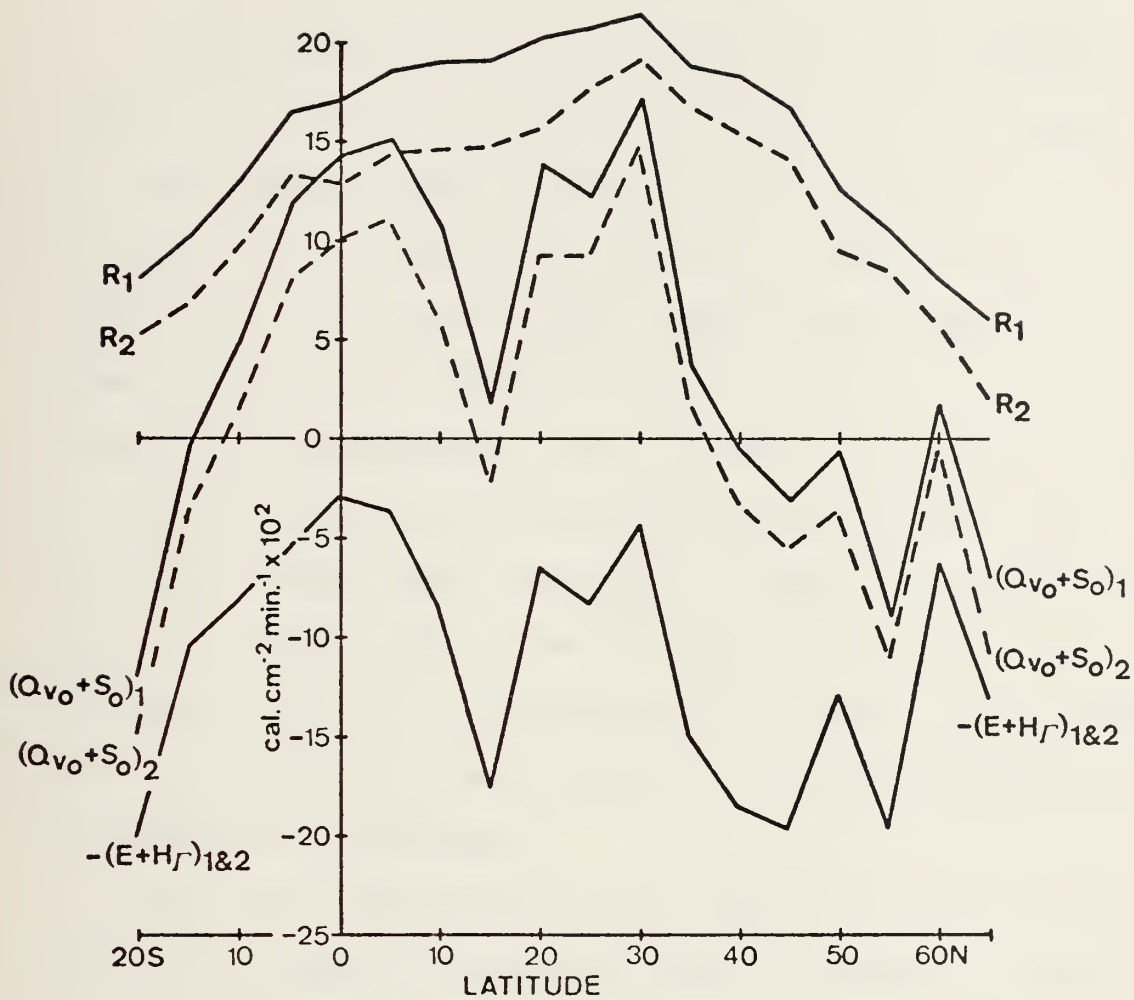


Figure 16. Distribution of R , $-(E+H_r)$ and of $Q_{vo}+S_o$ as a function of latitude for the two cloud-model cases. (solid curves represent the 2/3-CL case and dashed curves represent the full-CL case)

IX. CONCLUSIONS

The present work continues the use of the radiational two-layer cloud model adapted from Spaeth's mid-winter study to FNWC gridpoint data valid over the four meridians for 16 April 1974. The use of the 2/3-CL parameterization, as compared to the full-CL after Smagorinsky (1968), for the specification of cloud-layer amounts gave the best verification for the computed global albedo as a function of latitude when compared with observations from NIMBUS III satellite climatology comparable to that of 16 April 1974. The use of the 2/3-CL parameterization also gave good verification of computed long-wave flux to space when compared to the latitudinal distribution of the same element as given by satellite climatology.

The chief shortcoming of the computed global albedo versus the satellite measured albedo occurred in tropical latitudes (20S-20N). Here, it appears that cloud-elements do not behave as reflecting sheets for insolation but rather as focusing devices through the intra-cloud spaces. The use of 50-60% model cloud reflectances seems excessive in these latitudes. As a practical alternative it may be reasonable to tune the cloud reflectances until agreement of the computed global albedos with satellite measurements is achieved in the latitude range 20S-20N.

In the topics, all analyses are subject to data-sparsity and hence are largely dependent upon climatology and a relatively few radiosonde reporting stations. An apparent weakness in this study is that of overspecifying cloud-amounts through the use of Smagorinsky type formulas. This could be a result of inadequately resolved relative humidities, which in general might well be lower than inferred by the FNWC analyses.

LIST OF REFERENCES

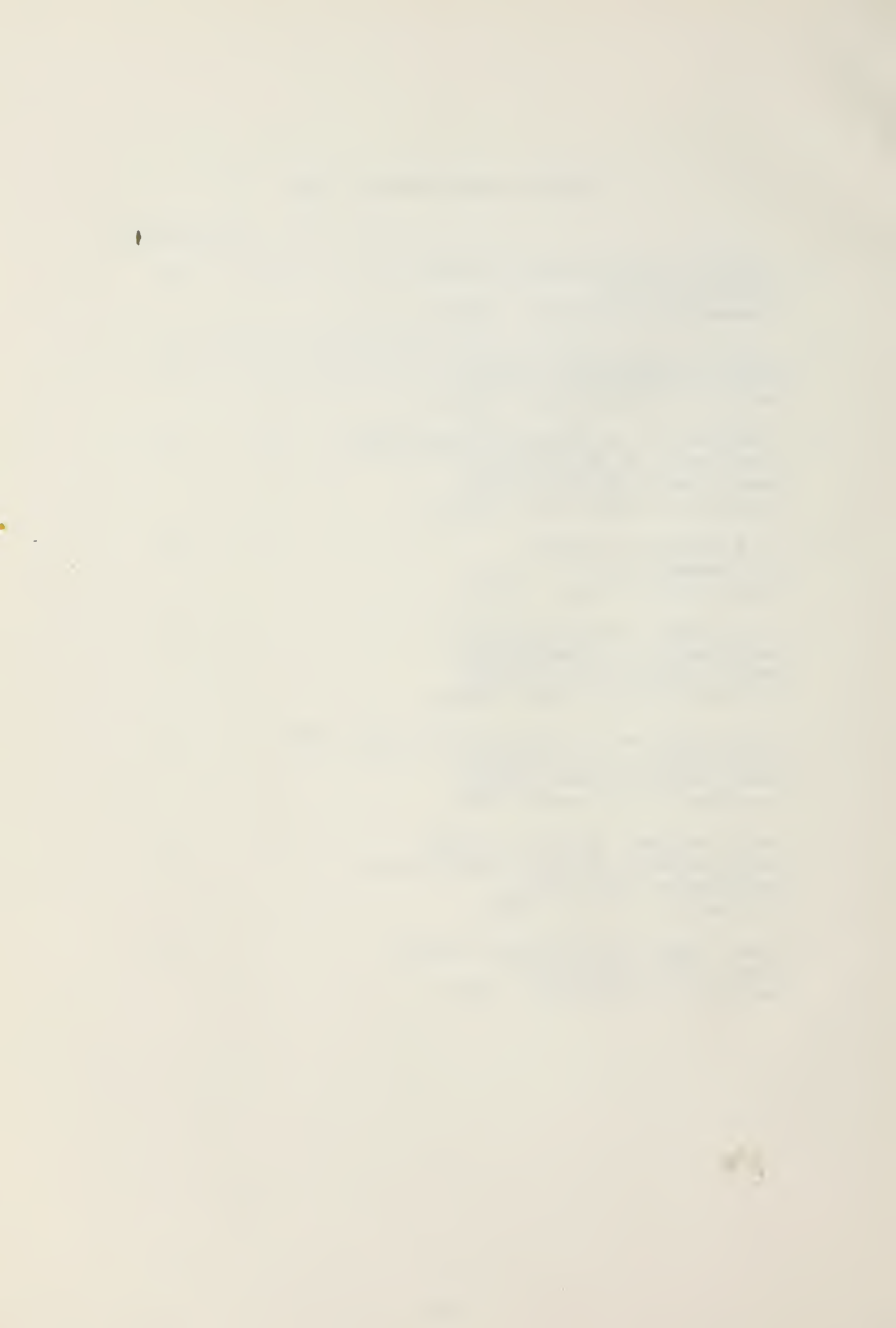
1. Arakawa, A., 1972: Design of the UCLA General Circulation Model, Numerical Simulation of Weather and Climate Tech. Rpt. No. 7, Department of Meteorology, University of California.
2. Beahan, T. W., 1975: Radiational Parameterization for the FNWC Primitive Equation Model Using Data Over the Oceans for 16 July 1974, M. S. Thesis, Department of Meteorology, Naval Postgraduate School, Monterey, California.
3. Budyko, M. I., 1958: The Heat Balance of the Earth's Surface, Leningrad, pp. 255 (Translated by N. A. Slepanova; translation distributed by U. W. Weather Bureau, Washington, D. C.
4. Coulson, K. L., 1959: Radiative Flux from the Top of Rayleigh Atmosphere, Ph.D. Dissertation, Department of Meteorology, University of California, pp. 60.
5. Dixon, W. J., 1973: Biomedical Computer Programs, University of California Press, pp. 773.
6. Fleagle, R. G., Businger, J. A., 1963: An Introduction to Atmospheric Physics, Academic Press, New York, pp. 346.
7. Hanson, K. J., 1971: Studies of Cloud and Satellite Parameterization of Solar Irradiance at the Earth's Surface, paper presented at the Miami Workshop on Remote Sensing, Miami, Florida, 29-31 March 1971.
8. Joseph, J. H., 1971: "On the Calculation of Solar Radiation Fluxes in the Troposphere," Solar Energy, Vol. 13, Pergamon Press, London, pp. 251-261.
9. Kaitala, J. E., 1974: Heating Functions and Moisture Source Terms in the FNWC Primitive Equation Models, paper presented at the Continuing Education Program for Meteorological Specialists, Naval Postgraduate School, Monterey, California, 29 April 1974.
10. Kesel, P. G., Winninghoff, F. J., 1972: "The Fleet Numerical Weather Central Operational Primitive-Equation Model," Monthly Weather Review, Vol. 100, No. 5.
11. Langlois, W. E., Kwok, H. C. W., 1969: Description of the Mintz-Arakawa Numerical General Circulation Model, Numerical Simulation of Weather and Climate Tech. Rpt. No. 3, Department of Meteorology, University of California.

12. Malkus, J. S., 1962: "Large Scale Interactions," The Sea, Vol. 1, Interscience Publishers.
13. Martin, F. L., 1972: Description of a Radiation Package for the Naval Postgraduate School General Circulation Model, Department of Meteorology, Naval Postgraduate School, Monterey, California.
14. Martin, F. L., 1974: Unpublished manuscript, Department of Meteorology, Naval Postgraduate School, Monterey, California.
15. Quinn, W. H., 1971: Studies of Parameterization of Solar Irradiance at the Earth's Surface, paper presented at the Miami Workshop on Remote Sensing, Miami, Florida, 29-31 March 1971.
16. Raschke, E., Von der Haar, T., Bandeen, W., Pasternak, M., 1973: The Annual Radiation Balance of the Earth-Atmosphere System during 1969-1970 from NIMBUS III Measurements," Journal of the Atmospheric Sciences, Vol. 30, No. 3, pp. 341-364.
17. Rodgers, C. D., 1967: "The Radiative Heat Budget of the Troposphere and Lower Stratosphere," Planetary Circulation Project Report N, A2, Department of Meteorology, Massachusetts Institute of Technology, pp. 99.
18. Sasamori, T., 1968: "The Radiative Cooling Calculation for Application to General Circulation Experiments," Journal of Applied Meteorology, Vol. 7, No. 5, pp. 721-729.
19. Smagorinsky, J., 1960: "On the Dynamical Prediction of Large Scale Condensation by Numerical Methods," Geophysical Monograph, No. 5, American Geophysical Union, Washington, D. C., pp. 71-78.
20. Smith, W. L., 1966: "Note on the Relationship Between Total Precipitable Water and Surface Dew Point," Journal of Applied Meteorology, Vol. 5, No. 5, pp. 726-727.
21. Spaeth, W. T., Jr., 1975: Heat Budget Parameterization for the FNWC Primitive Equation Model Using Data for 16 January 1974, M. S. Thesis, Department of Meteorology, Naval Postgraduate School, Monterey, California.

22. Von der Haar, T. H., Hanson, K. J., 1969: Absorption of Solar Radiation in Tropical Regions," Journal of the Atmospheric Sciences, Vol. 26, No. 4, pp. 652-655.
23. Von der Haar, T. H., Oort, A. H., 1973: "New Estimate of Annual Poleward Energy Transport by Northern Hemisphere Oceans," Journal of Physical Oceanography, Vol.3, No. 2, pp. 169-172.
24. Warner, D. W., 1974: Heat Budget Parameterization for the FNWC Primitive Equation Model Using Data for 16 October 1973, M. S. Thesis, Department of Meteorology, Naval Postgraduate School, Monterey, California.
25. Yamamoto, G., 1952: "On a Radiation Chart," Science Rpts of the Tohoku University, Series No. 5, pp. 9-23.

INITIAL DISTRIBUTION LIST

	No. Copies
1. Defense Documentation Center Cameron Station Alexandria, Virginia 22314	2
2. Library, Code 0212 Naval Postgraduate School Monterey, California 93940	2
3. Professor F. L. Martin, Code 51Mr Department of Meteorology Naval Postgraduate School Monterey, California 93940	4
4. LT William T. Meyers 208 South Hill Pilot Point, Texas 76258	2
5. Department Chairman, Code 51 Department of Meteorology Naval Postgraduate School Monterey, California 93940	1
6. Assoc. Professor R. L. Haney, Code 51Hy Department of Meteorology Naval Postgraduate School Monterey, California 93940	1
7. Naval Weather Service Command Naval Weather Service Headquarters Washington Naval Yard Washington, D. C. 20390	1
8. Fleet Numerical Weather Central Attn: Mr. Leo Clarke Monterey, California 93940	2



Thesis
M572
c.1

Meyers

Radiational parameterization for the FNWC primitive equation model using data over the oceans for 16 April 1974.

162231

Thesis
M572
c.1

Meyers

Radiational parameterization for the FNWC primitive equation model using data over the oceans for 16 April 1974.

162231

thesM572

Radiational parameterization for the FNW



3 2768 001 88309 3

DUDLEY KNOX LIBRARY